

**Synthesis and Characterizations of Molybdenum Doped Losod
Zeolite for Photocatalytic Dye Degradation and Hydrogen
Production**



By

Hamza Khawaja

(Registration No: 00000361972)

Department of Thermal Energy Engineering

U.S. Pakistan Center for Advanced Studies in Energy

National University of Sciences & Technology (NUST)

Islamabad, Pakistan

(2024)

**Synthesis and Characterizations of Molybdenum Doped Losod
Zeolite for Photocatalytic Dye Degradation and Hydrogen
Production**



By

Hamza Khawaja

(Registration No: 00000361972)

A thesis submitted to the National University of Sciences and Technology,
Islamabad,

in partial fulfillment of the requirements for the degree of

Master of Science in
Thermal Energy Engineering

Supervisor: Dr. Asif Hussain Khoja

Co-Supervisor: Dr. Mustafa Anwar

U.S. Pakistan Center for Advanced Studies in Energy
National University of Sciences & Technology (NUST)

Islamabad, Pakistan

(2024)

DEDICATION

To the culmination of relentless effort, fueled by the unwavering prayers of my mother, the exceptional support of my beloved wife, and the invaluable moral backing of my cherished colleagues.

ACKNOWLEDGEMENTS

All praise and thanks to Allah Almighty, who provided me with the power and skills to comprehend, learn, and complete my thesis report.

It gives me great pleasure to express my heartfelt gratitude to my research supervisor, Dr. Asif Hussain Khoja, for allowing me to join the Fossil Fuels Lab study group, USPCAS-E, NUST, Islamabad. I consider myself fortunate to have worked under his supervision. It was a combination of his patience, perseverance, guidance, and inspiration that enabled me to complete my research goals on time. He showed me the approach to conducting research and presenting the findings as clearly as possible.

My heartfelt gratitude goes to my dear Parents, whose unwavering support was a constant source of guidance, hope, and encouragement during this significant journey. I sincerely thank my friends and colleagues for their unwavering assistance and encouragement, which uplifted me in every possible manner.

THESIS ACCEPTANCE CERTIFICATE

Certified that final copy of MS Thesis written by Mr. Hamza Khawaja (Registration No. 00000361972), of U.S. Pakistan Center for Advanced Studies in Energy has been vetted by undersigned, found complete in all respects as per NUST Statutes/ Regulations/ Masters Policy, is free of plagiarism, errors, and mistakes and is accepted as partial fulfillment for award of Master's degree. It is further certified that necessary amendments as pointed out by GEC members and foreign/ local evaluators of the scholar have also been incorporated in the said thesis.

Signature: _____
[Handwritten Signature]

Name of Supervisor: Dr. Asif Hussain Khoja

Date: 24/10/2024

Signature (HOD): _____
[Handwritten Signature]

Date: 24/10/2024

Signature (Principal) _____
[Handwritten Signature]

Date: 30/10/2024

National University of Sciences & Technology
MASTER'S THESIS WORK

We hereby recommend that the dissertation be prepared under our supervision by **Hamza Khawaja** (Reg. No: 361972).

Titled: "Synthesis and Characterizations of Molybdenum Doped Losod Zeolite for Photocatalytic Dye Degradation and Hydrogen Production" be accepted in partial fulfillment of the requirements for the award of **MS Thermal Energy Engineering** degree with **(B+)** grade.

Examination Committee Members

1. Name: Dr. Rabia Liaquat

Signature: 

2. Name: Dr. Muhammad Hassan

Signature: 

Supervisor's name: Dr. Asif Hussain Khoja

Signature: 

Date: 24/10/2024

Co-Supervisor's name: Dr. Mustafa Anwar

Signature: 

Date: 25/10/2024

Dr. Asif Hussain Khoja
Head of Department

Signature: 

Date: 24/10/2024

COUNTERSIGNED

Date: 30/10/2024

Principal: 

CERTIFICATE OF APPROVAL

This is to certify that the research work presented in this thesis, entitled "Synthesis and Characterizations of Molybdenum Doped Losod Zeolite for Photocatalytic Dye Degradation and Hydrogen Production" was conducted by Mr. Hamza Khawaja under the supervision of Dr. Asif Hussain Khoja.

No part of this thesis has been submitted anywhere else for any other degree. This thesis is submitted to the Department of Thermal Energy Engineering in partial fulfillment of the requirements for the degree of Master of Science in Field of Thermal Energy Engineering Department of Thermal Energy Engineering National University of Sciences and Technology, Islamabad.

Student Name: Hamza Khawaja

Signature: 

Examination Committee:


a) GEC 1: Dr. Rabia Liaquat
Associate Professor, USPCAS-E, NUST

Signature: 

b) GEC 2: Dr. Muhammad Hassan
Associate Professor, USPCAS-E, NUST

Signature: 

Supervisor Name: Dr. Asif Hussain Khoja

Signature: 

Co-Supervisor Name: Dr. Mustafa Anwar

Signature: 

Name of HOD: Dr. Asif Hussain Khoja

Signature: 

Name of Principal: Prof. Dr. Adeel Waqas

Signature: 

AUTHOR'S DECLARATION

I Hamza Khawaja hereby state that my MS thesis titled "Synthesis and Characterizations of Molybdenum Doped Losod Zeolite for Photocatalytic Dye Degradation and Hydrogen Production" is my own work and has not been submitted previously by me for taking any degree from National University of Sciences and Technology, Islamabad or anywhere else in the country/ world.

At any time if my statement is found to be incorrect even after I graduate, the university has the right to withdraw my MS degree.

Name of Student: Hamza Khawaja

Date: Hamza Khawaja

v

PLAGIARISM UNDERTAKING

I solemnly declare that research work presented in the thesis titled "Synthesis and Characterizations of Molybdenum Doped Losod Zeolite for Photocatalytic Dye Degradation and Hydrogen Production" is solely my research work with no significant contribution from any other person. Small contribution/ help wherever taken has been duly acknowledged and that complete thesis has been written by me.

I understand the zero-tolerance policy of the HEC and National University of Sciences and Technology (NUST), Islamabad towards plagiarism. Therefore, I as an author of the above titled thesis declare that no portion of my thesis has been plagiarized and any material used as reference is properly referred/cited.

I undertake that if I am found guilty of any formal plagiarism in the above titled thesis even after award of MS degree, the University reserves the rights to withdraw/revoke my MS degree and that HEC and NUST, Islamabad has the right to publish my name on the HEC/University website on which names of students are placed who submitted plagiarized thesis.

Student Signature:



Name: Hamza Khawaja

Table of Contents

ACKNOWLEDGEMENTS	VIII
TABLE OF CONTENTS	IX
LIST OF TABLES	XI
LIST OF FIGURES	XII
LIST OF SYMBOLS, ABBREVIATIONS AND ACRONYMS	XIII
ABSTRACT	XIV
CHAPTER 1: INTRODUCTION	1
1.1 Background	1
1.2 Problem Statement	2
1.3 Research Hypothesis	4
1.4 Objectives of the study	5
1.5 Scope of the study	5
1.6 Flow chart	8
CHAPTER 2: LITERATURE REVIEW	10
2.1 Hydrogen as a Future Fuel	10
2.1.1 <i>Steam Reforming</i>	11
2.1.2 <i>Electrolysis</i>	12
2.1.3 <i>Bio-Photolysis</i>	15
2.1.4 <i>Thermochemical Process</i>	16
2.1.5 <i>Photolysis</i>	18
2.1.6 <i>Overview of all Hydrogen Production Technologies</i>	19
2.2 Photocatalytic Dye Degradation	20
2.2.1 <i>Photocatalytic Production of Hydrogen</i>	21
2.2.2 <i>Mechanism and Evolution Reaction</i>	22
2.3 Selection of Photocatalyst	23
2.3.1 <i>Coal Fly Ash and Biomass Fly Ash Overview</i>	24
2.3.2 <i>Structure and Composition</i>	26
2.3.3 <i>Blending Coal and Biomass Fly Ash</i>	26
2.4 LOS-Z Production and Structure	27
2.5 Tailoring the Properties of Selected Photocatalysts for H₂-Production	28
2.5.1 <i>Doping/Loading Effect</i>	29
2.6 Role of Sacrificial Agent	30
2.6.1 <i>Methanol</i>	30
2.6.2 <i>Ethylene glycol</i>	31
2.6.3 <i>Glycerol</i>	32

2.7	Role of Light Source	33
	CHAPTER 3: METHODOLOGY AND MATERIAL PREPARATION	35
3.1	Collection of Raw Materials	35
3.1.1	<i>Catalyst synthesis</i>	35
3.1.2	<i>Photocatalytic dye degradation</i>	37
3.2	Photocatalytic H₂ production	38
3.3	Material Characterizations	39
	CHAPTER 4: RESULTS AND DISCUSSION	40
4.1	Catalyst Characterization	40
4.2	Optoelectronic Properties	45
4.3	Photocatalytic reaction mechanism for dye degradation	56
4.4	Photocatalytic hydrogen evolution	61
	CHAPTER 5: CONCLUSIONS AND FUTURE RECOMMENDATION	66
5.1	Conclusions	66
5.2	Recommendations	66
	REFERENCES	68
	LIST OF PUBLICATIONS	77

LIST OF TABLES

Table 4.1: Band gap of the CFA-BFA blend, LOS-Z, 5% Mo@LOS-Z and 10% Mo@LOS-Z samples	49
Table 4.2: Rate constant (k) and R ² of the CFA-BFA blend, LOS-Z, 5% Mo@LOS-Z, and 10% Mo@LOS-Z samples	53
Table 4.3: Comparison of different studies of photocatalytic dye degradation	60
Table 4.4: Comparison of different catalysts used in photocatalytic H ₂ production	65

LIST OF FIGURES

Figure 1.1: Scope of the study	7
Figure 1.2: Flow chart of thesis	9
Figure 2.1: Hydrogen Production through Steam Methane Reforming [18]	12
Figure 2.2: Schematic representation of Hydrogen production through Electrolysis [22].	14
Figure 2.3: Production of Hydrogen through Biological Methods [24]	15
Figure 2.4: SI cycle for Hydrogen Production [28]	17
Figure 2.5: Hydrogen production technologies and their applications [33]	19
Figure 2.6: Schematic representation of photocatalytic hydrogen production [41].....	23
Figure 2.7: Properties of Photocatalyst for Hydrogen Production [43]	24
Figure 3.1: Schematic Diagram of catalyst synthesis	36
Figure 3.2: Experimental setup of photocatalytic dye degradation and hydrogen production	39
Figure 4.1: (a) XRD and (b) FTIR spectra of CFA-BFA blend, LOS-Z, 5% Mo@LOS-Z, and 10% Mo@LOS-Z	43
Figure 4.2: SEM analysis and (a1-d1) EDX analysis of CFA-BFA blend, LOS-Z, 5% Mo@LOS-Z, and 10% Mo@LOS-Z respectively. (e-f) Elemental mapping of 10% Mo@LOS-Z	45
Figure 4.3: (a) UV-vis and (b) PL spectra of CFA-BFA blend, LOS-Z, 5% Mo@LOS-Z and 10% Mo@LOS-Z	47
Figure 4.4: The band gap of (a) CFA-BFA blend, (b) LOS-Z, (c) 5% Mo@LOS-Z, and (d) 10% Mo@LOS-Z	49
Figure 4.5: Photocatalytic dye degradation of MB using (a) CFA-BFA blend, (b) LOS-Z, (c) 5% Mo@LOS-Z, and (d) 10% Mo@LOS-Z	51
Figure 4.6: (a) photocatalytic degradation vs irradiation time, (b) pseudo-first-order kinetics of synthesized samples.....	52
Figure 4.7: Catalyst dosage of (a) 0.5 mg mL ⁻¹ , (b) 1 mg mL ⁻¹ , (c) 2 mg mL ⁻¹ , and (d) % degradation efficiency of 10% Mo@LOS-Z in MB dye.....	54
Figure 4.8: Varying MB concentration (a) 2.5 ppm and (b) 7.5 ppm using 2 mg mL ⁻¹ catalyst dose	55
Figure 4.9: Reusability of 10% Mo@LOS-Z photocatalyst	56
Figure 4.10: Active radical trap test of 10% Mo@LOS-Z	57
Figure 4.11: Photodegradation mechanism of MB using 10% Mo@LOS-Z photocatalyst under visible lamp	59
Figure 4.12: H ₂ production of treated dye water during photocatalytic oxidation of methanol in the presence of (a) CFA-BFA blend, (b) LOS-Z, (c) 5% Mo@LOS-Z, and (d) 10% Mo@LOS-Z photocatalyst.....	61
Figure 4.13: Photodegradation mechanism of H ₂ using 10% Mo@LOS-Z photocatalyst under Xe lamp	64

LIST OF SYMBOLS, ABBREVIATIONS AND ACRONYMS

BFA	Biomass Fly Ash
CFA	Coal Fly ash
C _b	Conduction Band
FTIR	Fourier Transform Infrared Spectroscopy
H ₂	Hydrogen
LOS-Z	Losod Zeolite
Mo	Molybdenum
UV	Ultraviolet
V _b	Valence Band
MB	Methylene Blue

ABSTRACT

This research investigates the synthesis and application of Losod-zeolite (LOS-Z), a crystalline hydrated sodium aluminosilicate ($\text{Na}_{12}\text{Al}_{12}\text{Si}_{12}\text{O}_{48}\cdot x\text{H}_2\text{O}$) as a potential photocatalyst for dye degradation and H_2 production from dye-degraded water. The photocatalytic properties are enhanced by impregnating molybdenum (Mo) into LOS-Z (Mo@LOS-Z). XRD, FTIR, SEM, EDX, and elemental mapping were used to study the physiochemical properties of synthesized materials while UV-vis and PL were employed to explore the optoelectronic properties. The photocatalytic activities for dye degradation and H_2 production were evaluated using methylene blue (MB) under visible light irradiation. An enhancement in the efficiency of dye degradation (56% to 82%) and H_2 production rate was demonstrated due to the competitive photocatalytic performance of 10% Mo@LOS-Z compared to the pristine LOS-Z and CFA-BFA blend. It exhibited 2.5 times higher ($\sim 1200 \mu\text{mol g}^{-1}\text{h}^{-1}$) H_2 production than the LOS-Z ($\sim 480 \mu\text{mol g}^{-1}\text{h}^{-1}$) due to the synergistic effects of narrowed band gap and recombination rate. This study could pave the way forward into the synthesis of waste-derived photocatalysts for efficient dye degradation and H_2 production.

Keywords: *Dye degradation, Losod type Zeolite, Photocatalysis, H_2 production*

Chapter 1: Introduction

1.1 Background

A substantial increase in population and industry can be seen in the last few years, significantly elevating the quest for renewable and sustainable substitutes for energy to address global energy challenges and concerns. Hydrogen (H_2) brings a transformative pathway towards a greener future, addressing this problem, due to its high energy density, high energy conversion, large storage capacity, and versatile energy carrier [1, 2]. H_2 being considered an essential raw material, does not present naturally as a molecule [3]. Instead, several natural and synthetic materials, such as water, metal hydrides, formic acid ammonia, carbohydrates, and hydrocarbons can be converted into H_2 using different synthetic routes [4]. Over 96% of the world's H_2 production is from fossil reserves. Among these, 48% is formed from steam reforming, 30% from naphtha reforming, and 18% from coal gasification [5].

Unfortunately, most of the conventional H_2 production approaches result in significant energy consumption and environmental pollution [6]. Consequently, there is a prominent emphasis on novel technologies utilization from renewable resources, in tandem with rigorous global environmental protection standards, for H_2 production [7].

In many smaller projects, drinking water networks are used for H_2 production. However, it has become necessary to explore alternative water resources as this is an unsustainable approach for large H_2 production plants [8]. Reportedly, approximately 380 billion m^3 per year, with a 51% increase by the year 2050 global wastewater production

has been estimated [9]. The main contributor to water pollution is the textile industry because of the dyes dissolved in water bodies while also being a major consumer of freshwater, estimated at around 3-308 L kg⁻¹ [10, 11]. The textile industry frequently uses methylene blue (MB) dyes in their processes [11]. Therefore, using dye-degraded water for H₂ production is a sustainable option. MB dye is well-known for its deep blue colour, good solubility, and cationic properties. It exhibits major absorption of visible light, with a maximum absorption peak at around 664 nm which decreases with increasing irradiation in photocatalytic degradation. Resultantly, the dye is mineralised to CO₂ and H₂O as a result of the breakdown of its N-S heterocyclic structure. It also reduces the colour and toxicity of MB which can be further used for H₂ production [12]. Owing to its natural characteristics of high absorption capacity and removal percentage rate, MB is widely used for photocatalysis among other dyes [13]. Different studies have been performed on MB degradation and its utilization in H₂ production using catalysts [14-18].

1.2 Problem Statement

Excessive consumption of fossil fuel resources has played a significant role in advancing the current industrial society. As a result of this dependence, concerns regarding the adverse effects of fossil fuels on the environment are slim, leading to continuous usage and exhaustion of these scarce resources. It is important to note that governments, experts, and the public are beginning to understand the constant lingering demand for clean energy sources [1].

Regarding the textile industry, the primary concern is the production of wastewater from its operations. Unfortunately, large amounts of wastewater end up in landfills or

oceans, damaging our ecosystem. Therefore, utilizing wastewater in some value-added applications significantly lowers the harmful effects of unsustainable practices. Hydrogen production via wastewater treatment is an eco-friendly technique to utilize the wastewater instead of allowing it to pollute our water systems.

Among the various methods of photocatalytic hydrogen synthesis, this method is one of the most promising. This technology is useful in achieving future energy demands without causing environmental pollution as hydrogen is the clean energy carrier. This process involves a catalyst for the photochemical reaction to occur. It occurs when the energy absorbed is equal to or more than the bandgap energy [2]. When the photocatalyst absorbs a photon, an electron is excited and transfers from the valence band to the conduction band, leaving a hole in the valence band. This creates a radical anion that interacts with the electron acceptor while the hole at the valence band engages with the organic molecules to form hydroxide radicals [3].

Furthermore, the use of zeolites have paved the way for a new avenue for photocatalytic applications. Zeolites have a strong electric field around the cations and aluminosilicate framework which does not allow the recombination of the electron-hole pairs and enhances the charge transfer and separation [4]. The specificity of zeolites is that they can exchange cations, raising its surface acidity and non-uniform distribution of protons in the zeolite structure. These protons or Brønsted acidic sites are one of the sources for photocatalytic hydrogen production [5].

Nevertheless, to this date, these processes have failed to serve as a practical technique in real-life contexts despite their laboratory success. This is due to the limitations

surrounding the existing types of semiconductors including TiO_2 , ZnO , and SrTiO_3 . The performance of some of these semiconductors is limited by charge carrier recombination in the photo-excited electron-hole pairs and or photo-degradation. [6].

Scientists have focused on several approaches to solve these problems, among which is the incorporation of elements like Pt, Au, or Pd into the photocatalytic system to enhance light capturing and adjustment of redox potentials. These catalysts enhance charge separation, provide active sites, and decrease overpotential [7]. However, noble metals are rare and expensive, and thus there is a need to implement the use of cheaper metals like molybdenum, sulfur, selenium, or tellurium [8]. This research thesis seeks to address these issues and contribute to advancing commercially viable and environmentally friendly photocatalytic systems.

1.3 Research Hypothesis

According to the research hypothesis, incorporating a cheap transition metal, especially molybdenum as the heteroatom dopant in photocatalysis will improve the photocatalytic hydrogen production performance, stability, and cost-effectiveness [9]. This work is based on the understanding of the role of photocatalytic hydrogen production as a long-term solution to the world's energy problems. Transition metals are presented as viable alternatives because of their availability and advantages in price and efficiency.

The hypothesis deals with the limitations of photocatalysis, including their limitations on absorption of light, electron-hole pair recombination, and photo-corrosion. The goal of the research is to contribute to the manufacture of photocatalytic systems that are commercially feasible and ecologically sustainable by investigating the potential of

non-noble metals supported with losod-type zeolite as catalysts. Ultimately, this project aims to increase the viability of photocatalytic hydrogen generation as a sustainable energy alternative.

1.4 Objectives of the study

The current study seeks to advance photocatalytic hydrogen formation through photocatalytic dye degradation by creating innovative materials utilizing different formation techniques. With extensively scattered transition metals, such as Mo, the losod type zeolite photocatalytic activities are predicted to increase further. In this perspective, the objectives of this dissertation are further divided into three sub-objectives.

- ✓ Synthesized Mo@LOS-Z using a 2 step hydrothermal method
- ✓ Characterized morphological, compositional and structural properties of CFA-BFA blends, LOS-Z and Mo@LOS-Z using XRD, SEM, FTIR, and EDX techniques.
- ✓ Evaluated the photocatalytic performance of Mo@LOS-Z for the MB dye degradation under 35W Xe lamp
- ✓ Investigated the impact of Mo doping on the photocatalytic dye degradation and hydrogen production of LOS-Z
- ✓ Optimized the synthesis parameters of Mo@LOS-Z to achieve maximum efficiency for photocatalytic hydrogen production

1.5 Scope of the study

Based on the research accomplishments and current advancements in photocatalysis discussed above, it is demonstrated that there must be more studies and evident that there is a requirement for more study and development in the field of photocatalysis, specifically focusing on the production of hydrogen through photocatalytic dye degradation.

Blends-derived losod type zeolite was produced, dried at 100 °C to remove the moisture, and calcined at 700 °C to remove the volatile matter. The particular size of 0.2mm was obtained after grinding for smooth characterizations [10]. Different factors affected the required results including catalyst morphology, particle size, composition, reaction mechanism, reactor design, and light absorption efficiency [11]. These photocatalysts were synthesized with co-loading of Mo catalyst via physical mixing to improve conductivity and hydrogen yield and narrow the energy band gap. The photocatalyst was demonstrated for hydrogen production via water dissociation using sunlight under a nearby UV region and employing eco-friendly hole scavenger as methanol. The reaction mechanism was performed in a photo reactor, and the photocatalyst was tested. [Figure 1.1](#) below shows the scope of the research. XRD was used to test the photocatalyst for crystal structure, FTIR for different functional groups and chemical bonding, and SEM for morphology. Photochemical testing such as UV-viz for light absorption and band gap determination through Tauc plot, PL spectroscopy to study the charge recombination effect, and GC to see the hydrogen yield were performed.

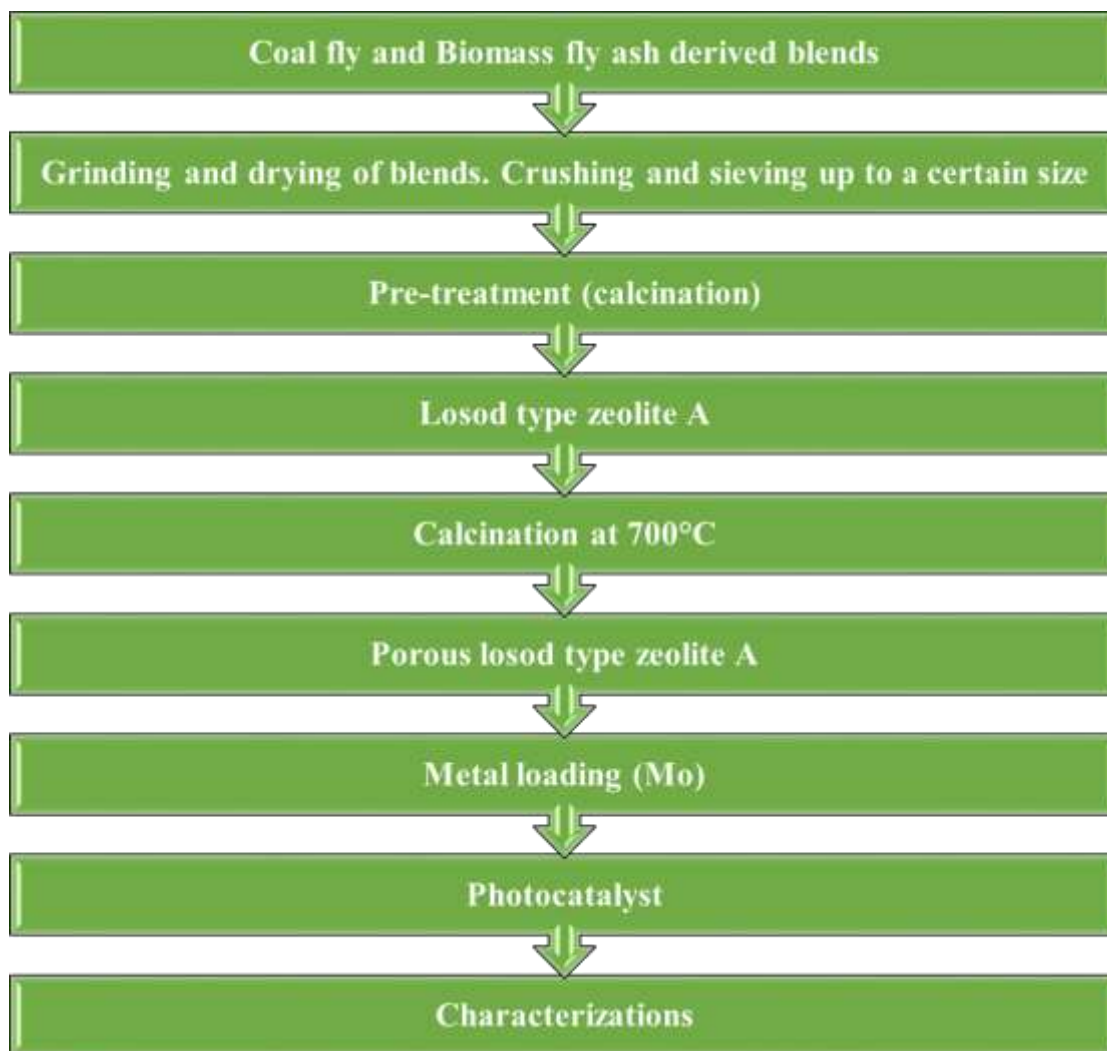


Figure 1.1: Scope of the study

1.6 Flow chart

The flow chart of the thesis is shown in [Figure 1.2](#). The aim of this study is to evaluate the synthesis of photocatalyst from waste material; blends of coal and biomass fly ash instead of discarding it and then employing elemental doping to improve the properties of photocatalyst. For this purpose, an existing literature review was studied. Mo@LOS-Z was prepared and then characterized using XRD, FTIR, and SEM, while UV-vis, GC and PL measured photocatalytic activity. The data was thoroughly reviewed from results and discussions.

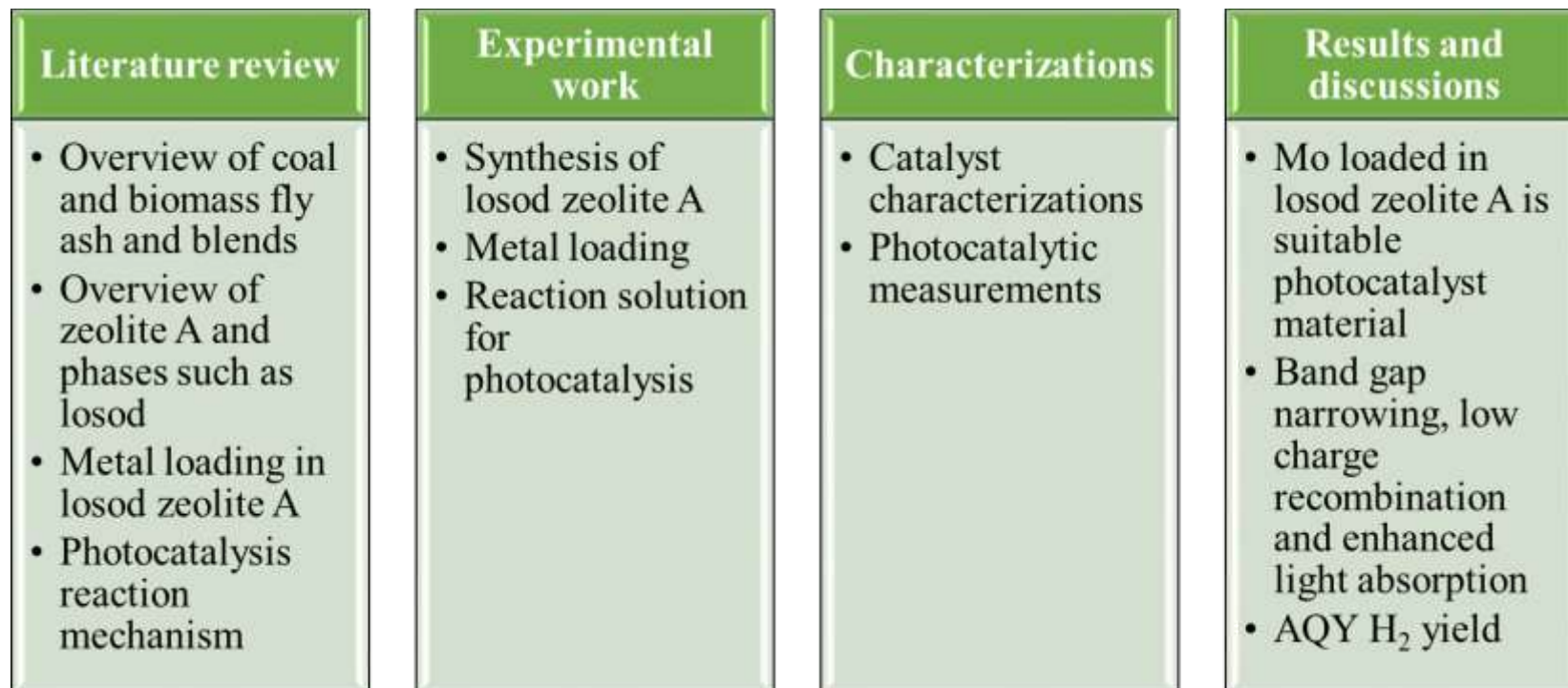


Figure 1.2: Flow chart of thesis

Chapter 2: Literature review

2.1 Hydrogen as a Future Fuel

Fossil fuel has been the main source of energy for many years. It has enabled the Industrial Revolution to occur, facilitating economic and technological developments. However, the excessive use of fossil energy resources has adverse effects on the natural environment, which threatens our planet. The most adverse consequence of fossil fuel use is the emission of GHGs, mainly carbon dioxide, during extraction, transportation and consumption. These are known to cause the greenhouse effect, increasing global temperatures and leading to climate change. This has serious ecological and economic concerns [12]. These drastic environmental effects include painting, pollution, deforestation, and destruction of habitats. Spills and accidents caused during the transportation of fossil fuels are known to cause catastrophes on both animals and human life. Additionally, supply systems of fossil fuels are volatile, due to the elements of risk and instability, especially if there are changes in the geopolitics or value factors in today's global economy [13].

Demands for H₂ production and storage would be paramount to address the energy requirements of the transport sector where the majority of the generated H₂ would be used to power homes, businesses, plants, and other industrial uses. Hydrogen, in its liquid and gaseous state, is produced in industrial processes. There are several approaches to free hydrogen from its compounds but to ascertain whether commercial production of hydrogen is financially viable would require further research and development [14].

Currently, hydrogen is manufactured from natural gas using the method known as steam-reforming accounting for 90-95% of hydrogen production. However, new methods are being studied, giving rise to clean fuel, as steam reforming releases carbon dioxide in large amounts [15]. The majority of these methods consist of splitting water into two components: hydrogen and oxygen. While some of these techniques are suitable for a hydrogen economy and safe for the environment, not all of them are. Some are explained below.

2.1.1 Steam Reforming

Steam methane reforming popularly known as SMR has become more significant since it was developed in 1930. Methane, mostly derived from natural gases, and other chemicals that are composed of hydrogen can be brought into hydrogen through the process of steam methane reforming (SMR). Hydrogenation of methane and steam occurs in SMR, which forms the products hydrogen, carbon monoxide, and carbon dioxide with the help of a catalyst. Later, carbon monoxide and dioxide are then removed by a process known as water-gas shift [16]. SMR is the most widely used technique for hydrogen generation – approximately 95% of global hydrogen production employs this method. This is so because its feed, natural gas which is the raw material used in processing this type of hydrocarbon is fairly available and cheap. In addition, SMR does produce hydrogen with a fairly high purity and general efficiency. Through the use of carbon capture and storage (CCS) technology or operation of the necessary process on renewable energy sources, SMR is in the process of reducing the overall carbon footprint [17]. The schematic diagram of the generation of hydrogen via SMR is shown in [Figure 2.1](#).

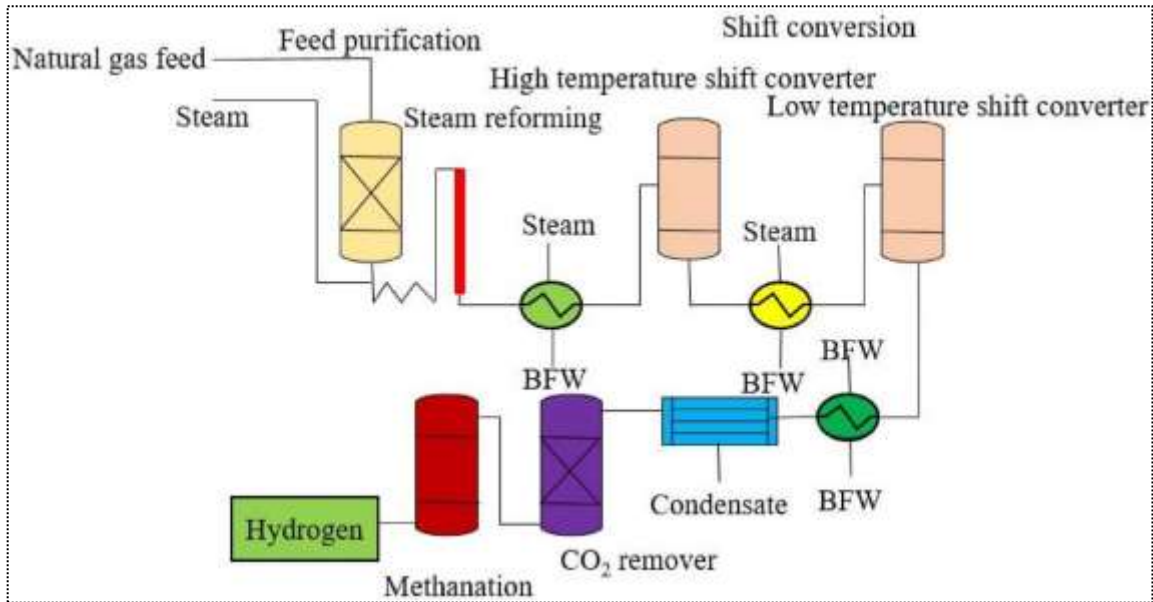


Figure 2.1: Hydrogen Production through Steam Methane Reforming [18].

Although this method is important, it has certain limitations.

- ✓ Due to the reversibility of the reaction, the generation of hydrogen is limited to the equilibrium conversion of methane.
- ✓ CO₂ is produced as a by-product, which contributes to climate change.
- ✓ Catalyst deactivation occurs due to carbon formation, limiting the catalyst's lifetime.
- ✓ Lastly, this process is reliant on the use of a fossil fuel (methane) [19].

2.1.2 Electrolysis

Many processes are known for the production of hydrogen which is a flexible and clean source of energy, for instance, electrolysis. Electrolysis can also be defined as the process through which electricity is used to decompose water into hydrogen and oxygen. Examples of electrolysis techniques that use the mentioned SOECs include the following: alkaline electrolysis solid oxide electrolysis cells polymer electrolyte membrane (PEM). There are several methods of electrolysis, but the most widely used method for hydrogen

generation is called alkaline electrolysis. It has a long operation history and ranging from well-known, but low efficiency, and no coordination with other units when it works under high pressure and temperature. PEM electrolysis seems to be more efficient than alkaline electrolysis mainly because it effectively operates under lower pressures and temperatures. It can therefore be used with other sources such as solar and wind energy and is most appropriate for small systems [20].

A relatively newer innovation in high-temperature technology, SOECs are advantageous in fuel cell and hydrogen production. Although they demonstrate very good possibilities for energy input flexibility and efficiency, they are still in the development stage and are expensive [21]. [Figure 2.2](#) shows a typical diagram for the electrolysis process of producing hydrogen.

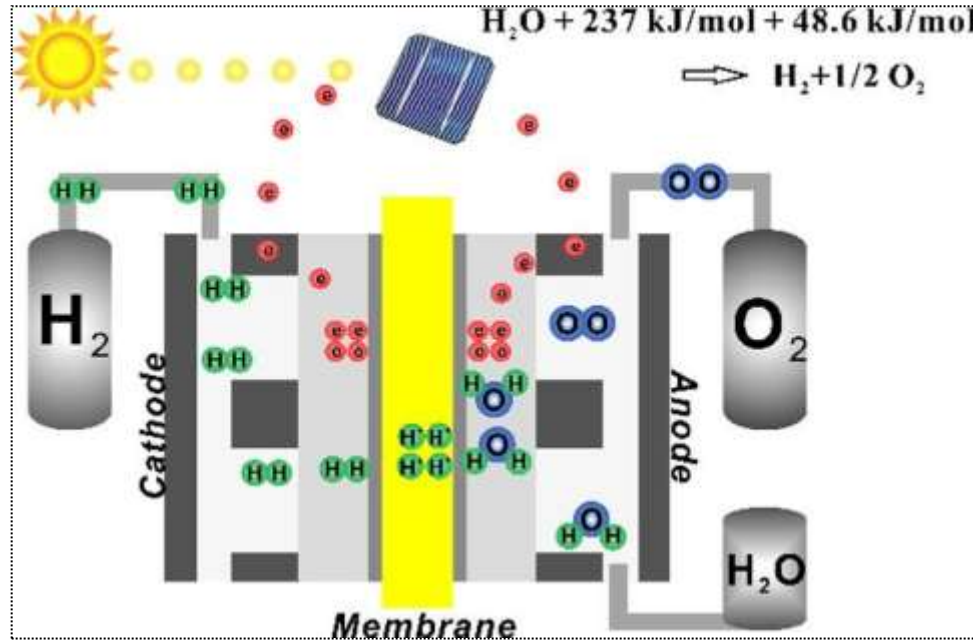
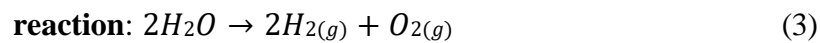
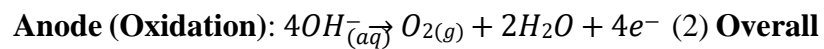
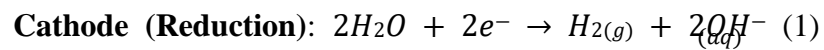


Figure 2.2: Schematic representation of Hydrogen production through Electrolysis [22].

The following equations represents how electrolysis works: oxygen is generated at the anode by the process of oxidation while, hydrogen is generated at the cathode through reduction.



Further, even though electrolysis generates hydrogen, it has been known that this is still an expensive method. It is also important that practical problems of the endurance and efficiency of the electrolysis equipment are also discussed.

2.1.3 Bio-Photolysis

Among them, the process of hydrogen production, known as biological hydrogen generation, holds the potential to produce renewable and sustainable hydrogen [23]. This makes it a better solution compared to that obtained by the industrial processes like the coal gasification as well as the SMR due to their adverse impacts on greenhouse gases. Here are some of the biological processes that are used in the production of hydrogen, as illustrated in Figure 2.3.

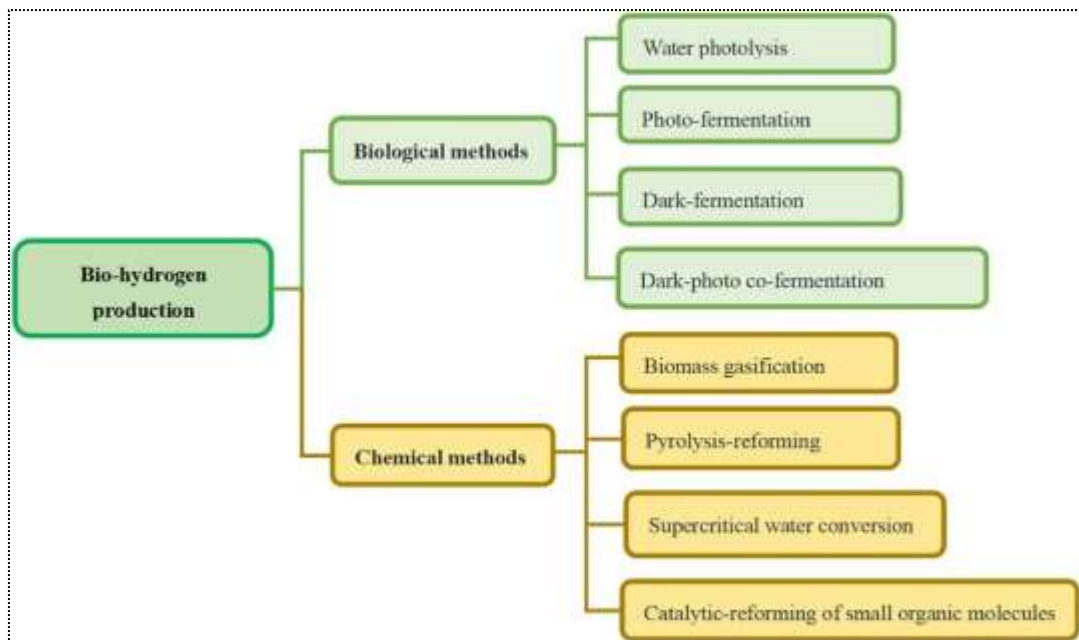


Figure 2.3: Production of Hydrogen through Biological Methods [24].

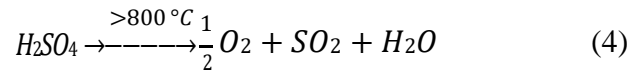
In oxygen-free conditions, there are specific groups of bacteria that convert organic compounds and are referred to as ‘dark fermentation’. The other observable outcome of bacterial activity is the disintegration of organic substrates as in the case of glucose [25]. Some bacterial species that are often utilized in this approach are Clostridium species and Enterobacter aerogenes. When light is present, so-called “photofermentation” yields

hydrogen in the form of gas by using photosynthetic microorganisms. Bacteria are known to metabolize organic electrons in the presence of light energy. An electrical current flows because the electrons are shifted to the anode part of the tissue. After that, water is decomposed into two components: hydrogen and oxygen with the help of electric currents [26].

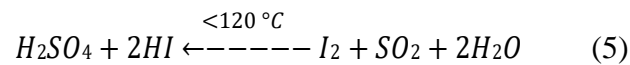
2.1.4 Thermochemical Process

Heat is used to manipulate a chain of chemical reactions which results in the production of hydrogen in thermochemical processes. Even though various types of thermochemical processes exist, one should admit that the potential of the sulfur-iodine (SI) cycle to produce large-scale commercial hydrogen seems to be the highest. Regarding Nadwa's current cycle, there are three stages within the SI cycle.

In the first step, we apply heat to sulfuric acid (H_2SO_4) to begin catalyzing the breakdown of sulfur and oxygen atoms and the creation of sulfur dioxide (SO_2), oxygen (O_2), and water (H_2O). This reaction needs to be of the order of $850^\circ C$ high because the enthalpy of this reaction is extremely positive.



In the second step, sulfur trioxide (SO_3) is created when oxygen oxidizes the SO_2 produced in the first step in the presence of a catalyst.



In the third step, sulfur dioxide combine with water to form sulfuric acid which can be recycled to the first step. It can use all sorts of heat, nuclear and solar, and fossil fuels and its theoretical efficiency is approximately 50% [27]. The hydrogen production from the SI cycle is shown in Figure 2.4 below.

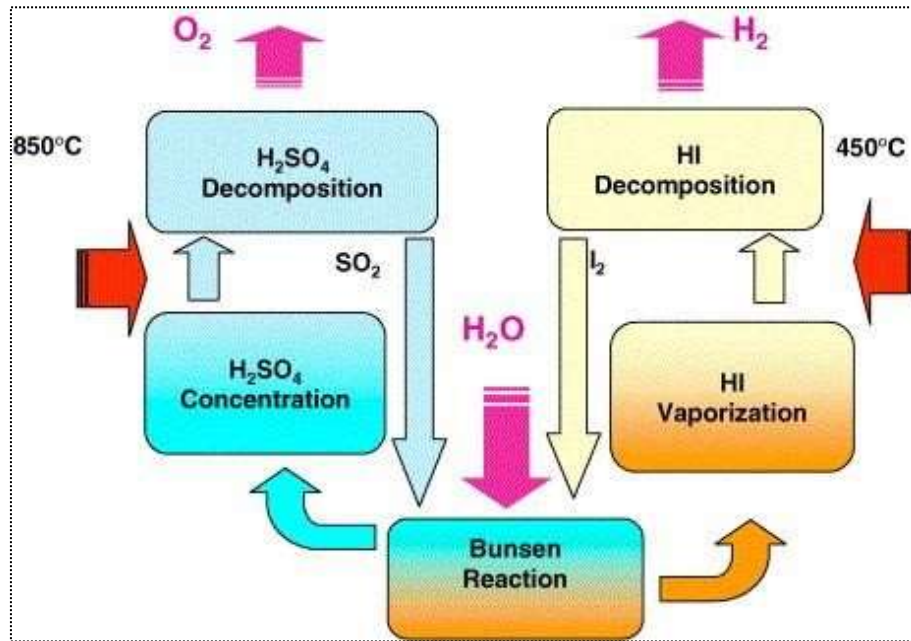


Figure 2.4: SI cycle for Hydrogen Production [28].

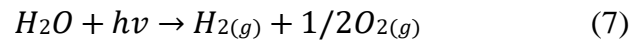
There are several obstacles and potential future developments in the thermochemical production of hydrogen [29]. One of the primary disadvantages of this approach is

- ✓ Its high energy requirements. When compared to other methods, the production of hydrogen through thermochemical processes may be more expensive because it requires higher temperatures and energy inputs.
- ✓ Issues with material compatibility and corrosion: It occurs when producing hydrogen through thermochemical processes. The elevated temperatures and acidic nature of certain chemicals utilized in these procedures may result in material compatibility issues and corrosion, shortening the lifespan of equipment and raising maintenance expenses.

- ✓ The complexity of thermochemical processes: It means that exact control over a range of parameters is required to optimize the yield of hydrogen. Lower yields or lower-quality hydrogen can be the result of process variability or errors.

2.1.5 *Photolysis*

The water-splitting photochemical synthesis that resulted in the production of hydrogen generated significant attention two decades back. In this process, photolysis or photodecomposition of water is done using photons to split the liquid into two components; hydrogen and oxygen [30]. Put differently, it is the process through which photon energy is transformed into chemical energy and then stored as hydrogen fuel.



When the potential difference is 1.23 eV or higher, this reaction takes place, which can be derived from the following eqs.

$$E = \Delta G_{(H_2O)}^o / 2N_A \quad (8)$$

Where the Gibbs free energy is 237. 2kJ/mol (2. 46eV) at room temperature and the value of Avagadro's constant which is equal to this particular reaction also has an enthalpy change of 2.96 eV. This number is equal to the wavelength of light at $\lambda = 420$ nm, which is in the blue light range of the electromagnetic spectrum. UV light is defined as light with wavelength $\lambda < 200$ nm, while the solar spectrum extends from the near-infrared to the near UV [31].

2.1.6 Overview of all Hydrogen Production Technologies

Figure 2.5 explains various ways of synthesizing hydrogen and different applications of hydrogen in different fields. From the aforementioned discussion, it can be deduced that the current popular technology in use is the thermochemical conversion. A majority of hydrogen is derived from nonrenewable sources such as fossil carbon feedstocks including coal, oil, and natural gas. Hydrogen can still be an innovative material in reaching carbonless energy though its production is still challenging without releasing carbons. This is why the energy sector has the rational to look for sustainable hydrogen production technologies that are expected to originate from sources other than carbon in the future [32].

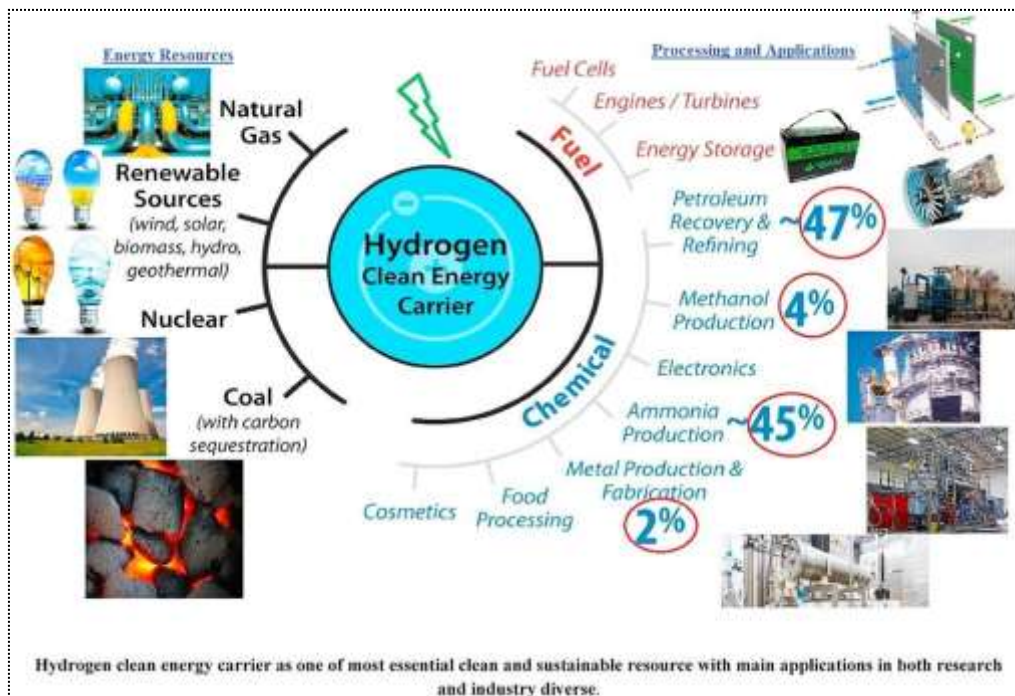


Figure 2.5: Hydrogen production technologies and their applications [33]

2.2 Photocatalytic Dye Degradation

Contamination of water is one of the most monumental environmental problems, especially in the textile and processing industry. The industry uses large volume of water, reportedly between 3 to 308 litres per kilogram of textiles produced and discharges high number of litres of polluted water comprising dangerous dyes and chemicals. They still remain significant for a modern world concerning the problem of environmental protection and facing new trends of hydrogen production. With the current global production rates of wastewater estimated to rise and reach around 380 billion cubic meters every year by 2050, there is need to look into various effective wastewater treatment approaches [34].

The photocatalytic dye degradation seems to be emerging as a good solution to this problem. This process involves a photocatalyst that facilitates a reaction through the action of light to decompose dye particles in wastewater. It begins when the energy of light that has been absorbed corresponds to the bandgap energy of the photocatalyst. A photon is absorbed bringing an electron from the valence band to the conduction band and forming an electron-hole pair. The electron in the conduction band reacts with an electron acceptor and forms a radical anion, while the hole within the valence band reacts with water molecules producing hydroxide radicals. These radicals are very active and can reduce the large size of organic dye molecules hence providing a good platform for other advanced water treatment processes [35].

The effectiveness of photocatalytic dye degradation depends upon such factors as nature of photocatalyst, light intensity and light wavelength, and characteristics of dye and wastewater. Some of the widely used photocatalysts includes titanium dioxide (TiO_2) and

zinc oxide (ZnO) because of their high oxidative ability, chemical inertness, and economical nature. When these photocatalysts are exposed to ultraviolet (UV) or visible light, electrons and holes are produced, which will cause the oxidation of dye molecules. The process can further be improved by increasing the surface area of the photocatalyst and the addition of dopants which aids in enhancing the light absorption capacity as well as separating the charges that are formed [36].

Beyond the environmental aspect, it is crucial to understand the significance of effective purification of wastewater through methods such as photocatalytic dye degradation. For clean energy solutions, treated wastewater can be a useful source for making hydrogen, which is a useful reactant. The conventional techniques of hydrogen production from wastewater are biological, adsorption, and oxidation which are capital and energy-comprehensive, as well as chemically demanding. Conventional photocatalytic systems can be overcome by using more advanced and efficient photocatalytic systems which have less chemical and energy demands [37].

2.2.1 Photocatalytic Production of Hydrogen

Photocatalysis is widely discussed in recent literature as it is based on two of the most available, clean, green, and natural energy resources available to mankind today. Thus, the photocatalytic generation of hydrogen has been considered as an effective solution to the challenges arising from the use of fossil fuels including overuse, low reserves, and the negative impact on the environment. As photocatalysis harness light energy and produces hydrogen cleanly without any greenhouse gas emissions, it can be beneficial to the environment as well as the economy [38].

2.2.2 Mechanism and Evolution Reaction

For a civilization to be considered sustainable hydrogen must presumably be produced from renewable sources. Photocatalytic water splitting ($\text{H}_2\text{O}/\text{H}_2 + 1/2 \text{O}_2$) is among the best methods of producing hydrogen from water by using solar power. After the Honda-Fujishima effect was first reported in 1972, research on this technology has been conducted in many countries. [Figure 2.6](#) illustrates the breakdown of water over a photocatalyst into oxygen and hydrogen [39].

To successfully produce hydrogen from water, three essential steps must be taken: The $\text{h}^+\text{-e}^-$ pairs are produced in the semiconductor when it absorbs light with energy equal to or higher than the bandgap energy of the semiconductor through the following processes: (i) absorption of light with similar or greater energy than the bandgap of the semiconductor to create the $\text{h}^+\text{-e}^-$ pairs; (ii) parting of photo charges by major transfer to the surface of semiconductor; and (iii) reaction with surface-adsorbed species. The photocatalytic activity of these materials is also affected by the recombination of the photo charges. Another common suppressing factor is back-reaction whereby the produced hydrogen and oxygen recombine with water to hinder photocatalytic water splitting [40].

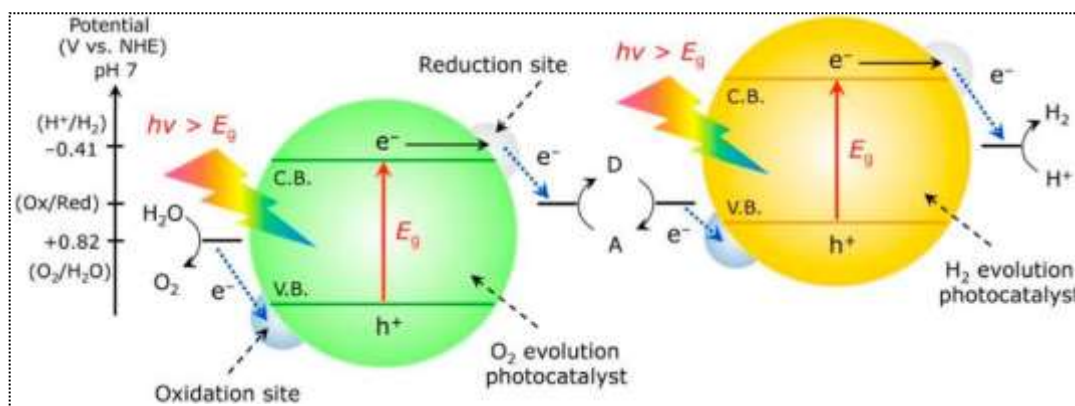


Figure 2.6: Schematic representation of photocatalytic hydrogen production [41].

2.3 Selection of Photocatalyst

The vast majority of catalysts are not efficient enough to harvest photons in the high-energy range, including UV and at times, portions of the visible light spectrum. One of the related restrictions is their band gap and the need to split water. Collection of energy within the visible part of solar spectra is critical to the utilization of solar energy. Photocatalytic research aims at finding a photocatalyst that is cheap, reactive, abundant, selective, and non-corrosive, and capable of operating on both the visible and ultraviolet portions of the electromagnetic spectrum. Over the years, many experiments have been carried out in the last few decades to create and intercalate new photocatalysts that could use both the UV and visible light spectrum to split water into hydrogen and oxygen. In some experiments, photocatalysts were tested in previous experiments using UV radiation and numerous materials displayed high quantum efficiencies [42].

However, the photocatalysts available in the market today present one major problem in that their efficiency is often very low. For the process to be efficient it has to have several factors, these include the band gap that will allow maximum use of solar spectrum, correct

placement of CB and VB so that oxidization and reduction reactions happen, stability at redox state, low cost of production and operation, reusability, availability in plenty, no vulnerability to corrosion, and suitability for large scale production. Figure 2.7 lists the basic requirements for photocatalysts for hydrogen generation as follows:



Figure 2.7: Properties of Photocatalyst for Hydrogen Production [43].

2.3.1 Coal Fly Ash and Biomass Fly Ash Overview

Coal fly ash and biomass fly ash are phosphate-silicate glass particles which are produced as a result of combustion processes in power plants and other industrial plants. These wastes, despite being classified as waste, have great potential uses such as in

construction products, for the improvement of soil structure, and for the extraction of rare earth metals. The knowledge of the characteristics and application of coal and biomass fly ash is important [44], especially when considering their combined use in innovative blends.

Coal fly ash is a byproduct that results from the combustion of coal in thermal electricity generation plants. Worldwide, the generation of coal fly ash alone is more than 750 million tons per annum with China, India, and the USA as the main producers. This ash mainly contains fine particles, the chemical composition of which includes silica, alumina, and iron oxides, thus it is well utilized in cement and concrete industries. Nevertheless, the management of coal fly ash results in land degradation and water pollution due to the leaching of heavy metals and toxic elements [45].

The usage of coal has triggered the recycling procedure possibility of the fly ash of coal in different areas. In construction, it is applied as a SCM which can be incorporated into the concrete to increase the durability of the concrete structures [46]. Further, coal fly ash has potential uses in the fabrication of geopolymers and zeolites, materials that could be used for environmentally friendly applications such as environmental cleanup and as catalysts. Nonetheless, a considerable amount of coal fly ash is not presently used, thereby highlighting the need to develop additional applications to assist in its beneficial reuse [47].

Biomass fly ash is a by-product of biomass combustion which includes agricultural residues and wood chip and municipal solid wastes. However, the production of biomass fly ash has been on the rise as countries look to biomass for renewable energy. For example, Pakistan produces about 220 billion tons of biomass and municipal solid waste in a year, thus the prospect of biomass fly ash production is significant [48].

Biomass fly ash contains many beneficial minerals like calcium, potassium, and magnesium, among others, suggesting that the material can be used to enhance the fertility of the soil and the output of the crop. The other difference between the two is in the content of toxic heavy metals in which biomass fly ash has lesser amounts and thus can be used for agricultural purposes safely [49].

2.3.2 *Structure and Composition*

Coal fly ash and biomass fly ash therefore characteristically have different chemical compositions and physical properties or structures thus their appropriate uses. The coal fly ash commonly consists of SiO_2 , aluminum oxide (Al_2O_3), iron oxide (Fe_2O_3), and small amounts of calcium oxide (CaO). Most of the fuller particle shapes are generally spherical and amorphous in nature [50]. On the other hand, fly ash obtained from biomass power plants comprises calcium oxide (CaO), silicon dioxide (SiO_2), potassium oxide (K_2O), and magnesium oxide (MgO). The ashes of biomass are constituted by particles with more capillary irregular surfaces and more porous than fly ash and containing higher proportions of organic remains [51].

2.3.3 *Blending Coal and Biomass Fly Ash*

The incorporation of coal fly ash with biomass fly ash is of paramount importance in the course of preparing Losod Zeolite (LOS-Z) mainly because the two types of ash have unique characteristics. It was noticed that mineralogical composition of the fly ash disposed of at the studied power plants contains high proportion of silica (SiO_2) associated with aluminum oxide (Al_2O_3) that are crucial for formation of zeolite structures. When mixed with biomass fly ash rich in nutrient substances, the blend provides a suitable chemical

environment for the formation of zeolite. As a result, this synergy facilitates the crystallization process and the generation of highly effective adsorption and ion exchange capacities for LOS-Z [52].

2.4 LOS-Z Production and Structure

The production of LOS-Z was achieved using a hydrothermal treatment process, a method renowned for its efficiency and effectiveness in synthesizing crystalline zeolites. Hydrothermal treatment involves the reaction of raw materials in an aqueous solution at elevated temperatures and pressures, facilitating the formation of highly ordered crystalline structures. This method is particularly advantageous for producing zeolites due to its ability to control the crystal size, purity, and uniformity of the final product [10].

In this research, a blend of coal fly ash and biomass fly ash was subjected to hydrothermal treatment. The high silica (SiO_2) and aluminum oxide (Al_2O_3) content in coal fly ash, combined with the calcium oxide (CaO) and other nutrients in biomass fly ash, created a favorable chemical environment for zeolite synthesis. The hydrothermal conditions facilitated the dissolution of these oxides and their subsequent reorganization into the zeolite framework, ensuring a high degree of crystallinity and optical properties for LOS-Z.

LOS-Z, which is otherwise called Linde Type A (LTA) zeolite, consists of a carnal framework of cubes and contains a high degree of porosity [53]. This structure consists of a three-dimensional network of SiO_4 and AlO_4 tetrahedral, linked by oxygen atoms. The basic structural units are the sodalite cages or beta cages, defined as truncated octahedral formed by 24 tetrahedral siting at vertices. These cages are linked by double four-ring

(D4R) units to form a more extensive three-dimensional rectangular grid with a unit cell [54]. The unit cell of LOS-Z has a lattice parameter of approximately 12.75 Å [55].

The blending of coal fly ash and biomass fly ash played a crucial role in the successful synthesis of LOS-Z. The high silica and alumina content from coal fly ash provided the necessary precursors for the zeolite framework, while the presence of calcium oxide and other minerals from biomass fly ash contributed to the stabilization and crystallization process. The balanced chemical composition achieved through blending ensured that the hydrothermal treatment conditions were optimized for zeolite formation, leading to a product with superior structural and functional properties.

2.5 Tailoring the Properties of Selected Photocatalysts for H₂-Production

The structure and properties of LOS-Z significantly influence its performance as a photocatalyst for hydrogen production. The effectiveness of LOS-Z in photocatalytic applications is affected by factors such as crystallinity, pore size distribution, surface area, and the presence of functional groups. These properties can be meticulously controlled to optimize photocatalytic activity.

LOS-Z has a cubic crystalline structure with high order which gives a high surface area with regular pore size [56], crucial for effective photocatalytic reactions.

The presence of surface roughness and oxidation functional groups is found to improve the photocatalytic activity of LOS-Z. These functional groups can act as nucleation sites for the growth of semiconductor particles like TiO₂ or ZnO so that the particles are uniformly dispersed through the entire matrix and have good interfacial

adhesion. This is important in the formation of heterojunctions, which enhances the charge separation process and at the same time reduces recombination rates hence increasing the efficiency of hydrogen production [57].

The addition of coal fly ash and biomass fly ash during the preparation of LOS-Z results to a balanced chemical composition that is useful in photocatalytic reaction. The high silica and alumina content of fly ash produced from the combustion of coal provide the needed framework of the structure while the calcium with other nutrient content in fly ash produced from the burning of biomass are effective in the stabilisation and crystallisation processes [58]. This synergy results in a zeolite with enhanced structural properties and a higher density of functional groups, which are crucial for efficient photocatalytic hydrogen production.

2.5.1 Doping/Loading Effect

Incorporation of some other elements or compounds into LOS-Z can dramatically increase its photocatalytic activity. This process is defined as the process of adding new elements within the zeolite structure or on the outer shells to enhance the zeolite properties. Doping can change the electronic properties of the zeolite, increase the number of active sites, and promote the interaction between zeolite and reactants. Loading normally refers to the deposition of photocatalytically active nanoparticles including metal oxides and noble metals on the outer surface of the zeolite to improve the adsorption of light and its separation into charges [59].

Doping and loading are crucial for optimizing the photocatalytic activity of LOS-Z. By carefully selecting the dopants and loading materials, it is possible to tailor the

zeolite's properties to specific photocatalytic applications, such as hydrogen production, pollutant degradation, and water splitting. These modifications can lead to improved efficiency, higher reaction rates, and better stability of the photocatalyst. The impact on photocatalytic properties is discussed below:

Doping and loading dependencies of LOS-Z, exposure makes it possible to use a greater portion of the spectrum, including the visible one. This enhances the photocatalytic processes and rate better by using or absorbing more light [60].

Specifically, the introduction of the dopants and loaded nanoparticles leads to an increase in the number of active sites on the surface of the zeolite which in turn improves reactivity. Increased active site results in enhanced photocatalytic reaction rates thus enhancing the photocatalytic performance [61].

2.6 Role of Sacrificial Agent

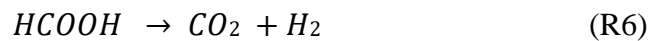
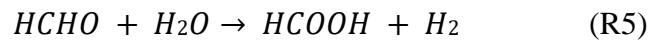
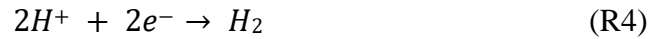
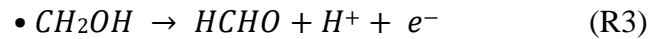
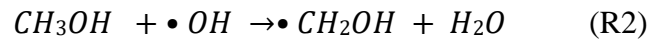
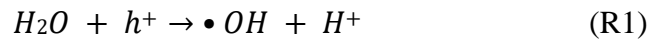
In this study, it is revealed that the most frequently used sacrificial reagents for oxide, carbon, and sulfide photocatalysts is methanol. The following is a brief description of some of the sacrificial agents mentioned above [62].

2.6.1 Methanol

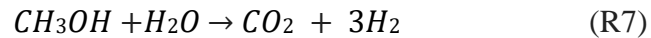
In photocatalytic hydrogen production, methanol is taken to be the benchmark molecule. Being regarded as the best active electron donor, newly developed materials are usually evaluated with this substance [63].

When compared with a water molecule which has a polar bond and a dipole moment of 1. For example, in the case of methanol, the fragment has a less polar dipole moment equal to 1.69D. Moreover, the presence of methanol dissolved in water reduces the hydrogen bonding between water molecules and thus opens the water structure for photochemical cleavage. It is the strong oxidizers popularly referred to as holes that force the splitting of water and the formation of hydrogen gas, which is represented as H₂ [64].

The reaction mechanism for methanol is given as follows.



The overall reaction is written as

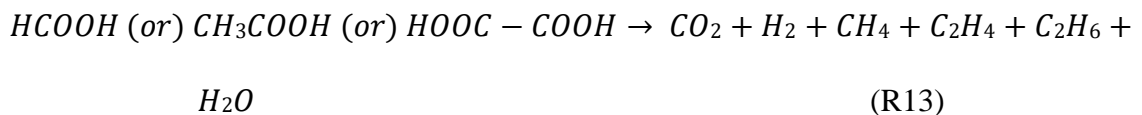
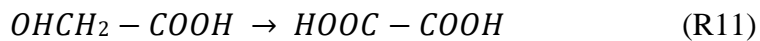
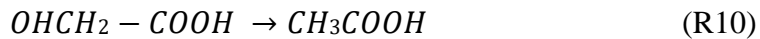
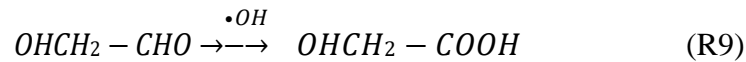
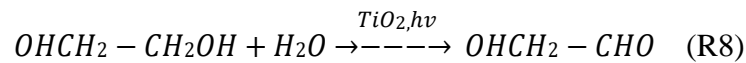


2.6.2 Ethylene glycol

The maximum values of hydrogen production were obtained while the overall mineralization values in this particular case had reached their maximum points, and among

the intermediates that were analyzed, tendencies similar to that of hydrogen production were evident. The maximum value of CO₂ is observed at the range corresponding to the maximum values of methanol and ethanol. However, even though it generates less hydrogen than ethanol, ethylene glycol mineralization rates are significantly higher. This is because, unlike ethylene glycol, other hydrocarbons such as ethane and methane possess reduction products. Also, in this case, the use of a pure sacrificial agent leads to little or no photocatalyst deactivation [65].

The reaction mechanism for ethylene glycol is given below.

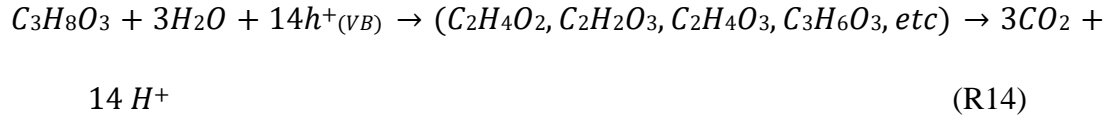


2.6.3 Glycerol

In fact due to the size of the glycerol molecule and its viscosity it is not possible to have 100% (v/v) sacrificial agent therefore its approach towards the catalyst surface is restricted. Due to the fact that glycerol is a complex alcohol other intermediates may be

produced which are difficult to predict. The formation of some compounds has been observed such as acrolein, acetone, glyceraldehyde, glycolaldehyde, ethanol, acetic acid, methanol, CO₂, CO, acetol, acetaldehyde and ethanol [66].

The reaction mechanism for glycerol is given as



2.7 Role of Light Source

Analyzing the experimental results, it is possible to increase the efficiency of photocatalytic water splitting: increasing the light intensity of radiation with energies higher than the activation threshold. Currently, there are two models describing the UV-photon flux and the photocatalytic reaction. The half-order regime, however, is regarding higher intensities and the rate of recombination is usually predominant and does not affect the rate of reaction to a great extent. The spectrum of adsorption for the catalyst has a threshold equal to the band energy, with the change in the rate of reaction as a function of the wavelength in the figure below [67].

When heterogeneous photocatalysis occurs then the required energy source can be calculated in terms of the band gap energy of a photocatalyst such as TiO₂ $\lambda \leq 387$. The method of luminescence of excited atoms or molecules with the electron transition in the excited higher states of atoms or molecules to the ground state of the atoms or the molecules with the simultaneous emission irradiations is the basic physical phenomenon of all

irradiation sources. Arc lamps, incandescent lamps, fluorescent lamps, and lasers are some of the classifications of lamps that are classified based on the working principle [68]. The substantial energy savings are the main benefit of using a UV-LED lamp.

Specifically, LEDs are more advantageous as less expensive, compact, lightweight, and highly efficient radiation sources in comparison with the traditional light sources. They also work at lower temperatures compared to the other types of refrigeration systems. Another form of irradiation source that can yield monochromatic light additionally with the restricted emission profile is a UV LED. This represents a remarkable improvement over the traditional mercury vapor lamps and is already within a sphere of visible LEDs. If the likes of visible light LEDs are anything to go by, it is expected that their efficiency will increase in the following years and if incorporated in photocatalytic water treatment, the increase in efficiency will also be greatly realized [69].

Chapter 3: Methodology and Material Preparation

3.1 Collection of Raw Materials

ASTM coal fly ash and biomass fly ash were collected from Fauji Power Plant Ltd., Sodium hydroxide (NaOH) pellets, sodium aluminate (NaAlO_2), molybdenum (99.5%, <150 μm), ethylenediaminetetraacetic acid disodium salt (EDTA, 98.5-101.5%), L-Ascorbic Acid (99%), Iso-propanol (IPA, 99.8%), and Cupric nitrate trihydrate (puriss. p.a., 99-104%) were purchased from Sigma Aldrich. MB dye (dye content ~82%) was obtained from SD Fine Chem. The precursors acquired were not prepared preliminary and were of analytical grade quality.

3.1.1 Catalyst synthesis

LOS-Z was prepared by a 2-step hydrothermal treatment method. To synthesize zeolite, 30 g of CFA-BFA blend powder was introduced into a 5 M NaOH solution (ACS reagent) in a 700 mL beaker. The non-stop stirring at 300 RPM using a magnetic stirrer at 100 °C maintained the dissolution temperature. Afterwards, filtration using a Whatman filter paper having a pore size of 0.2 μm , a clear solution was separated from the mixture. Next, 100 mL of NaAlO_2 solution was added to the clear filtrate to adjust the molar ratio to $\text{SiO}_2/\text{Al}_2\text{O}_3 \approx 1$, $\text{Na}_2\text{O}/\text{SiO}_2 \approx 1-2$, and $\text{H}_2\text{O}/\text{Na}_2\text{O} \approx 40$ for LOS-Z synthesis. The solution was again stirred for 30 min at 500 RPM at room temperature. The obtained milky solution was left overnight for 12 h to help the gel formation and aging. The aged sample was then kept in Teflon autoclaves (heat-resistant templates) and kept in an oven under variable crystallization temperatures and time. The optimized temperature (90-95 °C) and

time (1.5-2.5 h) were used to synthesize LOS-Z. After two-step crystallization temperature, the saturated solution was kept at room temperature to facilitate crystal growth for the next 12 h. DI water was used to filter and wash out the precipitates to remove excess Na ions. The product was then dried at 100 °C for 12 h [42].

Mo@LOS-Z (5 wt% and 10 wt%) were synthesized using an impregnation method in ethanol. Initially, pure Mo was added to 100 mL of ethanol to create a solution. For the 5 wt% Mo@LOS-Z catalyst, 2.5 mg of Mo and 47.5 mg of LOS were used while 5 mg of Mo and 45 mg of LOS were used for 10 wt% Mo@LOS-Z. The respective amounts of Mo and LOS were added to ethanol and stirred for 3 h. The solid residue was calcined at 700 °C for 5 h after overnight drying at 120 °C [43]. The synthesis of Mo@ LOS-Z is shown in Figure 3.1.

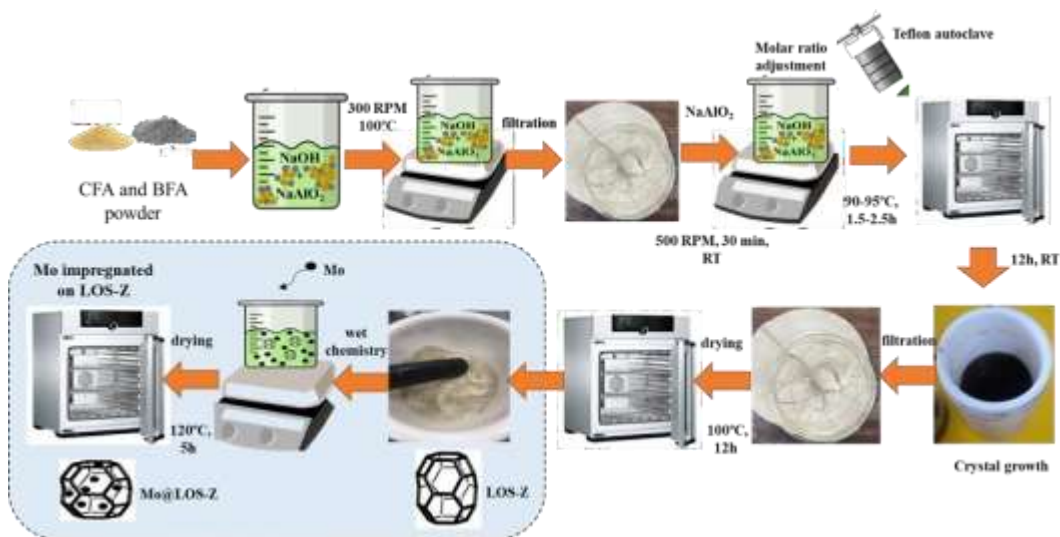


Figure 3.1: Schematic Diagram of catalyst synthesis

3.1.2 Photocatalytic dye degradation

Catalysts CFA-BFA blend, LOS-Z, 5% Mo@LOS-Z, and 10% Mo@LOS-Z photocatalysts were used for different experiments with a catalyst dose of 2 mg mL⁻¹ and 5 ppm (5 mg mL⁻¹) MB solution. These conditions were selected based on both literature and the hit-and-trial approach. Among all the photocatalysts, 10% Mo@LOS-Z exhibited better photocatalytic performance comparatively.

After 75 min, the samples for photocatalytic degradation were examined using UV-vis spectroscopy and results were analyzed at 664 nm (max) [44]. The source of visible light used to measure the photocatalytic degradation was a 35 W Xenon lamp having an intensity of 20 mW cm⁻² with a 6000 K colour temperature [45]. The solution (3 mL) was taken after every 15 min intervals. The concentrations of residual organic compounds were measured using a UV-vis at the maximum absorbance wavelength. Using the following Eq. 9, the photodegradation efficiency (%DE) was computed [73]:

$$\%DE = \frac{A_0 - A}{A_0} \times 100 \quad (9)$$

Where the initial concentration of MB and the concentration that is left over are represented by A_0 , respectively.

Moreover, different parametric studies were performed using different catalyst dosages and MB concentrations and reusability analysis.

3.2 Photocatalytic H₂ production

For the photocatalytic H₂ production test, 100 mg of photocatalyst was dissolved in a 50% v/v methanol-containing aqueous solution. The suspension was purged with N₂ gas in the dark for 30 min and then illuminated using 35 W of Xenon lamp under continuous stirring. Using a syringe, 10 mL of gas was extracted every half an hour (the total time of reaction was 3 h). To analyze the products, a system of gas analysis consisting of a gas chromatograph (GC-2010 Pro by Shimadzu Japan) fitted with a thermal conductivity detector (TCD) column (RT-MS5A, 30 m × 0.32 mm ID, 30 μm) was used. The experimental setup for photocatalytic dye degradation and H₂ production is presented in [Figure 3.2\(a-c\)](#). The first experiment in [Figure 2\(a\)](#) comprised dye degradation of MB solution in the presence of light exposure. The degradation efficiencies of four samples were calculated using UV-vis spectrometry. The degraded dye water was tested for H₂ application (experiment 2) in [Figure 3.2\(b-c\)](#) and subjected to GC chromatography to calculate H₂ production.

The experimental setup for photocatalytic dye degradation and hydrogen production is presented in [Figure 3.2](#).



Figure 3.2: Experimental setup of photocatalytic dye degradation and hydrogen production

3.3 Material Characterizations

To determine the structure and purity of the synthesized powders, XRD were recorded on a D8-Advanced Bruker, Germany instrument using Cu K radiation at $\lambda = 0.15418$ nm and a 2θ angle range of 20° - 80° . The morphology of the samples was determined using the TESCAN MIRA3 of Oxford Instruments INCAx-act, model 51-ADD0007, as well as the elemental mapping and field emission scanning electron microscopy (FESEM). Samples were sonicated in an ethanol solution for 20 minutes before the FESEM and then placed on a glass slide for examination. The photocatalytic activities of the catalyst, as well as the dye degradation, were measured using a Shimadzu UV-3600 Plus spectrophotometer. As a visible-light source, a 35 W Xenon lamp having an intensity of 20 mWcm^{-2} was used for photocatalytic dye degradation and subsequently hydrogen evolution. To identify functional groups and chemical bonds, FTIR analyses was performed. The equipment model used was Cary 630 FTIR (Agilent Technologies, USA). The recombination effect of e^-h^+ was examined by the photoluminescence emission (PL) at the excitation wavelength of 325 nm using HORIBA LPS221B.

Chapter 4: Results and Discussion

4.1 Catalyst Characterization

The crystallographic phases of different materials synthesized are shown in [Figure 4.1\(a\)](#). The XRD spectrum of the CFA-BFA blend constituted the characteristic peaks of both the parent materials due to their physical blending without any chemical change. The major peak at $2\theta = 26.5^\circ$ represents SiO_2 (PDF#46-1045), while the minor peaks are at $2\theta = 31^\circ$ and $2\theta = 33^\circ$ for Al_2O_3 (PDF#46-1131) and Fe_2O_3 (PDF#16-0653) respectively. These metal oxides exhibited properties that favour zeolite formation and catalyst synthesis [47].

The XRD of LOS-Z confirms the formation of different phases of zeolite including zeolite A (a metastable state) and LOS-Z which is thermodynamically more stable than zeolite A. The pattern displays characteristic peaks of zeolite A (PDF# 039-0222) at 2θ of 20° and 27.1° corresponding to the (210) and (212) respectively [48]. However, the conversion of zeolite A to LOS-Z phase ($\text{Na}_{12}\text{Al}_{12}\text{Si}_{12}\text{O}_{48}\text{xH}_2\text{O}$) with (PDF# 31-1269) can also be observed, suggesting that the CFA-BFA blend consists of multiple components other than Si and Al, e.g. Ca and Mg, that are related closely to the LOS-Z production [49, 50].

The characteristic peaks of LOS-Z are observed at 2θ of 23.9° , 26.5° , and 33.1° corresponding to the (211), (103), and (401) respectively [48]. However, the transformation of zeolite A phases into LOS-Z can be minimized by removing Ca and Mg content from the precursors [49]. This transformation can be further explained by using Oswald and Van

Santen's hypothesis based on non-equilibrium thermodynamics which has shown that the total entropy production is minimized during a phase change by following the "law of successive transformations" [51]. In this case, zeolite A is initially formed and is further converted into LOS-Z with the 2 steps hydrothermal treatment at 95 °C [49]. Thus, the given statement explicates the formation of zeolite A, a metastable state [52] that tends to transform thermodynamically into LOS zeolite.

The XRD pattern of 5% Mo@LOS-Z indicated additional peaks of Mo (PDF# 78-0390) at 40.5°, 58.6°, and 73.7° corresponding to the (110), (200), and (211) respectively. This confirmed the successful impregnation of Mo while the characteristic peaks of LOS-Z were maintained. A slight shift in the peak position of LOS-Z from 27.1° to 26.9° was observed due to the distortion in the crystal lattice. The impregnation of Mo into a LOS-Z matrix altered the crystal lattice causing expansion within the lattice and modifying the bond angles in the LOS-Z structures [53]. 10% Mo@LOS-Z also shows the same pattern as 5% Mo@LOS-Z except for the more prominent Mo peaks that can be observed with an increasing Mo loading. There is a noticeable shift observed from 26.9° to 26.7°, representing greater distortion as a result of more Mo concentration.

The FTIR spectra of all the synthesized samples are shown in [Figure 4.1\(b\)](#). The spectra clearly show the transition of the CFA-BFA blend to LOS-Z after synthesis. [54]. The peak appearance at 2095 cm⁻¹ (N=C=S) can be assigned to the cyanide-containing compounds present in traces in the CFA-BFA blend [55]. The major peak corresponds to the vibrations of Si-O stretching with wavenumber 1090 cm⁻¹ [56]. Additionally, stretching vibrations of C=O at 1420 cm⁻¹ and its bending plane at 880 cm⁻¹ evidence the presence of carbonate compounds (CaCO₃) in the CFA-BFA blend [54, 57]. A slight peak at 678 cm⁻¹

confirms the existence of CaSO_4 (S-O bending) due to the presence of CFA [54]. In LOS-Z, the asymmetric stretching in CFA-BFA blend at 1047.27 cm^{-1} (T-O asymmetric stretching) has changed to a low frequency of 962 cm^{-1} , which is a prominent characteristic of the framework of zeolite A [58, 59]. The peak at 962 cm^{-1} corresponds to the T-O-T (Al or Si) tetragonal stretching vibration's characteristic peak. This shift indicates that the possible reaction between the vitreous components of the ash and the alkaline activator (NaOH) formed the LOS-Z structure. This implies that the framework structure of the LOS-Z produced may have a lower Si/Al ratio than the feedstock material because some of the Si in the Si-O-Si bond has been replaced by Al for the Si-O-Al bond. A similar peak-like CFA-BFA blend can also be observed at 673 cm^{-1} (T-O symmetric stretching) corresponding to quartz [42]. The characteristic peaks for bicyclic vibrations in a tetrahedron exist at 663 cm^{-1} majorly for zeolite A [60]. In general, the asymmetric stretching mode of the vibrations common to all zeolites occurs between 950 and 1250 cm^{-1} [61]. The FTIR spectra of 5% and 10% Mo@LOS-Z represent the Mo-O peak by the presence of an absorption band below 1000 cm^{-1} . A small peak present at 673 cm^{-1} is the same as the peak in zeolite A spectra while the peak at 905 cm^{-1} is attributed to the Mo-O stretching vibrations [62]. It can be seen that the Mo-O peak in the 10% Mo@LOS-Z is broader as compared to the 5% Mo@LOS-Z and a clear shift in the spectra indicates increased interaction between Mo and LOS-Z by increasing the concentration of Mo that promotes the coordination with the LOS-Z [63].

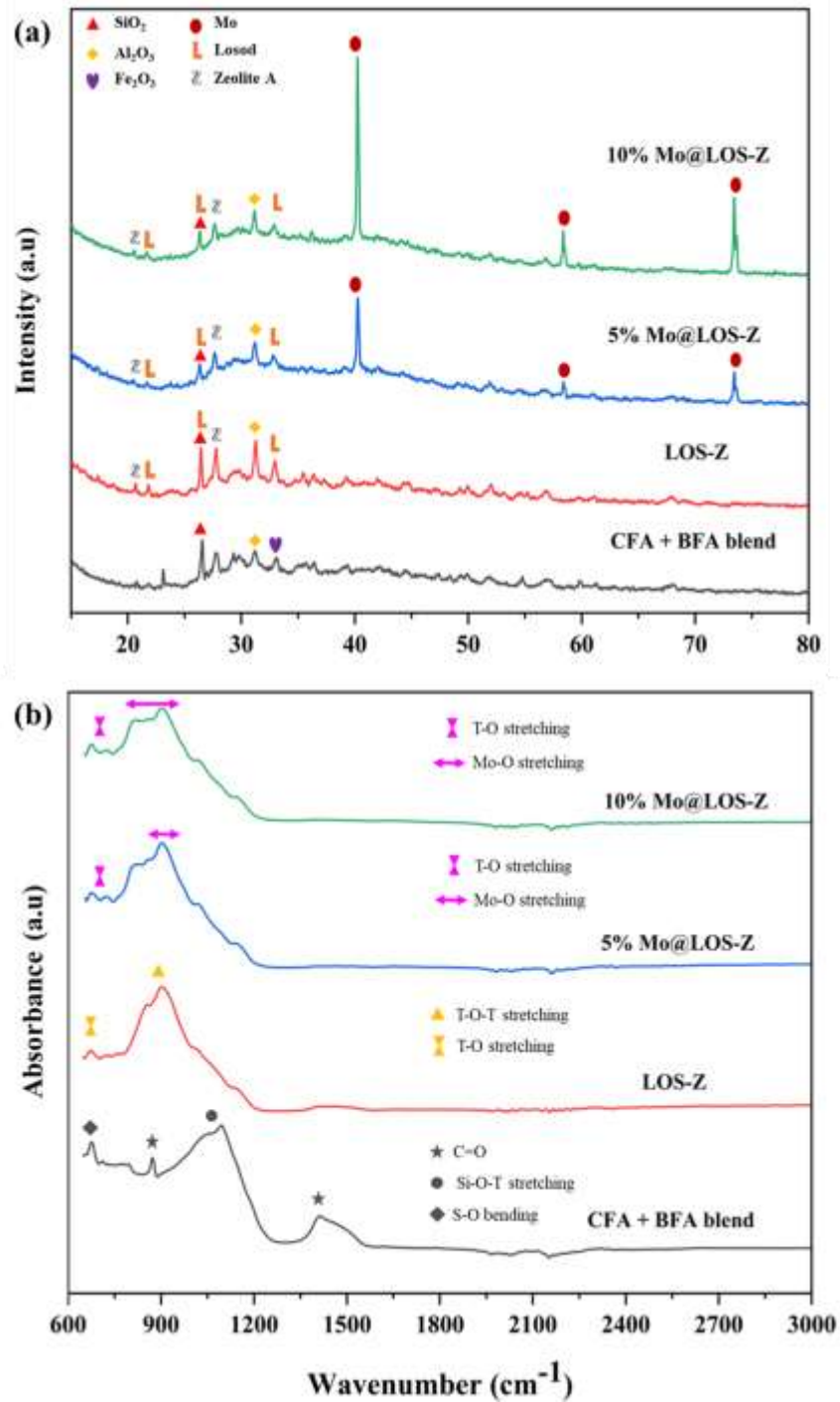


Figure 4.1: (a) XRD and (b) FTIR spectra of CFA-BFA blend, LOS-Z, 5% Mo@LOS-Z, and 10% Mo@LOS-Z

The SEM images of the CFA-BFA blend, LOS-Z, 5% Mo@LOS-Z and 10% Mo@LOS-Z are shown in [Figure 4.2](#). SEM micrographs revealed that the CFA-BFA blend sample in

Figure 4.2(a) is amorphous, hollow, and constitute fractured surfaces. However, Figure 4.2(b) showed agglomerates due to the conversion of the CFA-BFA blend into LOS-Z with a few mild crystals of zeolite A present in the matrix. These agglomerates are described as interpenetrating crystallites [64]. In contrast, 5% and 10% Mo@LOS-Z in Figure 4.2(c-d) are roughly spherical and show scattered Mo particles over the surface. In 10% Mo@LOS-Z, the distribution of Mo particles is uniform over the LOS-Z support in comparison to other samples, which can enhance the photocatalytic performance. Microscopic examination reveals that silicate and aluminosilicate predominate in the CFA-BFA blend as shown in Figure 4.2(a1). It demonstrates that at a particular spectrum, the CFA-BFA blend contained 9.81% aluminium, 12.77% silicon, 45.18% oxygen, 19.58% calcium, and other minute peaks of several elements. In Fig. 4.2(b1), LOS-Z showed 12% aluminium, 13.23% silicon and 52.92% oxygen. The high percentage of oxygen with Al and Si revealed the successful formation of aluminate and silicate respectively (building blocks of zeolite structure). Figure 4.2(c1) confirmed the presence of 5.53 wt% Mo with Si, Al and Ca present in significant amounts and their proportions were slightly changed due to the modification in crystal structure while introducing Mo. In Figure 4.2(d1), the Mo concentration increased to 7.58 wt% expectedly and the higher deposition of Mo on the LOS-Z matrix occupies the positions of other elements causing the reduction in their concentration [65]. Figure 4.2(e-f) illustrates the elemental mapping of 10% Mo@LOS-Z which shows the dispersion of different particles including Si, Al, O, Mo, and Ca on its surface. The Mo particles are concentrated and well dispersed on LOS-Z, confirming its uniform distribution as shown in Figure 4.2(f).

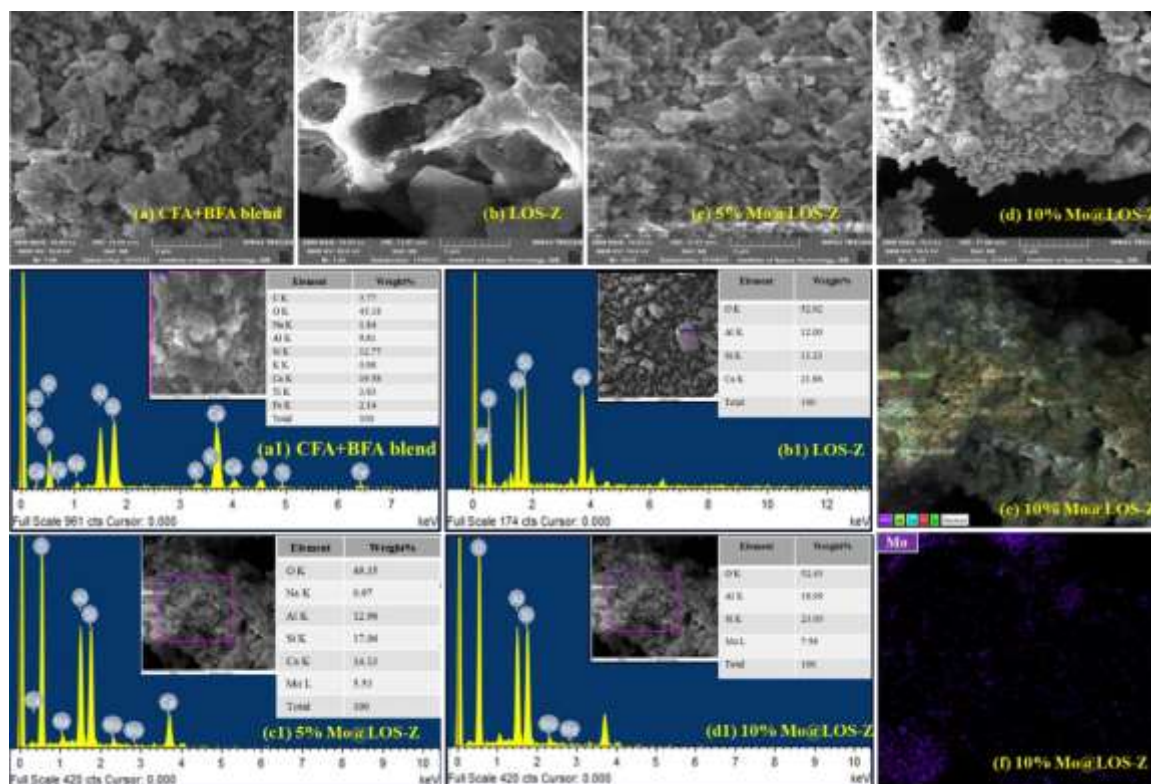


Figure 4.2: SEM analysis and (a1-d1) EDX analysis of CFA-BFA blend, LOS-Z, 5% Mo@LOS-Z, and 10% Mo@LOS-Z respectively. (e-f) Elemental mapping of 10% Mo@LOS-Z

4.2 Optoelectronic Properties

The optimization of the material's photocatalytic properties plays a significant role in its interaction with light and generating EHP [66, 67]. A material having a lower band gap will produce a large amount of EHP and vice versa. Similarly, the recombination effect has an inverse relation with EHPs. These characteristics of a material will decide its compatibility with applications such as dye degradation and H₂ evolution via photocatalysis.

The UV-vis spectra shown in [Figure 4.3\(a\)](#) are measured for synthesized samples in the range of 240 nm-600 nm. The study was conducted in the dispersed solution and it can

be observed that a broad absorption band stretches from 240 nm to 300 nm. It can be seen that the absorption of photocatalyst is increased in the order of CFA-BFA blend < LOS-Z < 5% Mo@LOS-Z < 10% Mo@LOS-Z. Hence, 10% Mo@LOS-Z has the highest absorption, indicating the maximum contribution in enhancing photocatalytic performance as evident from XRD and SEM as well. The recombination effect, mobility and entrapment of charge carriers of EHPs for LOS-Z, 5% Mo@LOS-Z and 10% Mo@LOS-Z are studied by PL spectroscopy shown in [Figure 4.3\(b\)](#). The electrons are excited by using monochromatic light of 325 nm (visible region). By absorbance of photons in the valence shell results in the creation of EHP. The intensity has a direct relation with the recombination of EHP [68]. The CFA-BFA blend has a higher intensity than LOS-Z, 5% Mo@LOS-Z and 10% Mo@LOS-Z indicating the highest recombination of EHP. This is due to the rough and minimal active sites (as evident from SEM) for EHP separation that could help in separating the charge carriers therefore increasing the recombination rate. Similarly, for LOS-Z the large cavities trap charge carriers reducing recombination compared to the CFA-BFA blend and supporting better charge separation. As soon as Mo is introduced into the LOS-Z matrix, a decreasing trend in the intensity was observed that suppressed the recombination of the charge while enhancing the composite's photocatalytic efficiency. Mo is an efficient electron acceptor by forming the mid-gap states [69]. As the concentration of Mo is increased, the excited electrons are captured by Mo atoms therefore preventing recombination with holes. The morphological studies also showed the availability of multiple sites of Mo for charge-trapping across the LOS-Z matrix. This indicates that optimum loading is a proven strategy to suppress the charge

carriers [70] resulting in 10% Mo@LOS-Z photocatalyst being a good candidate in this study.

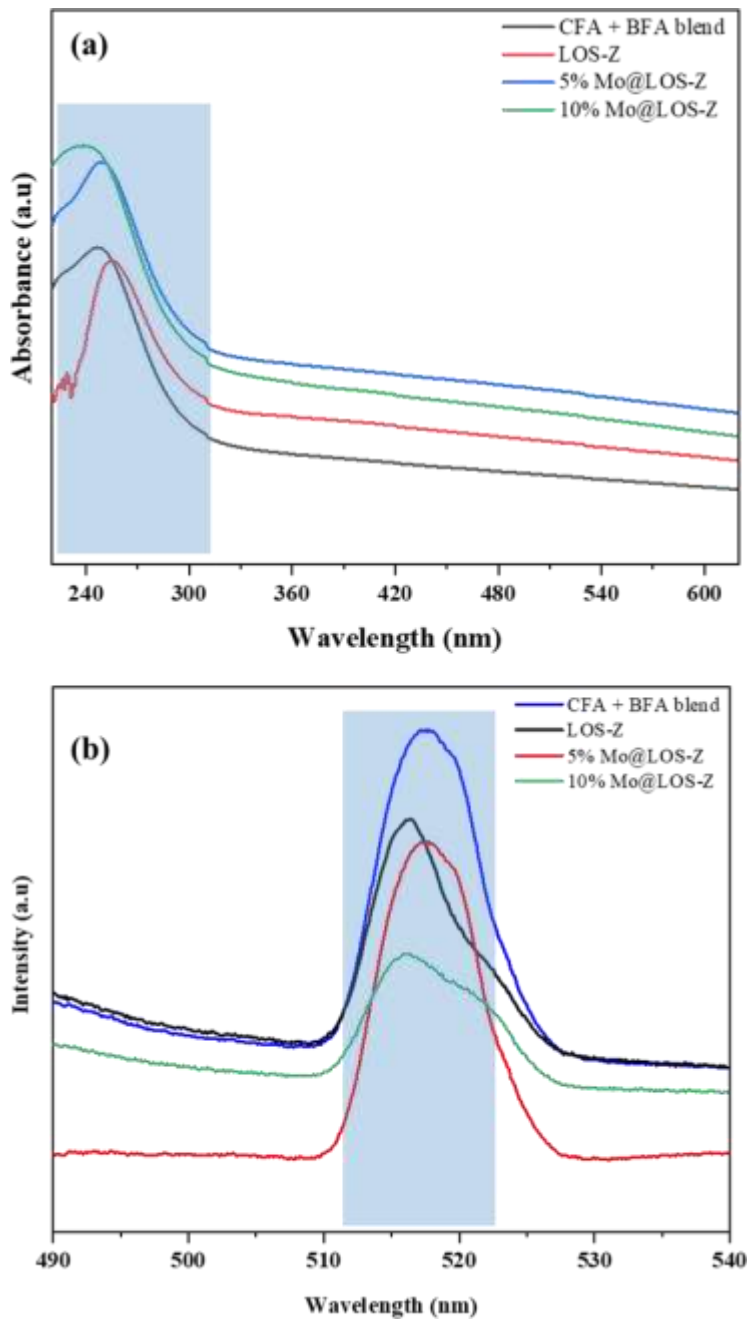


Figure 4.3: (a) UV-vis and (b) PL spectra of CFA-BFA blend, LOS-Z, 5% Mo@LOS-Z and 10% Mo@LOS-Z

Moreover, the UV-vis absorption spectrum calculates the band gap using the direct band Tauc's equation as given in Eq. 10 and listed in Table 4.1.

$$(ah\nu)^{1/n} = K(h\nu - E_g) \quad (10)$$

Here α , h , ν , K , n , and E_g represent the adsorption coefficient, Planck's constant, frequency, energy independent constant, nature of transition (direct or indirect band gap), and optical band gap energy respectively [71]. In this study, the direct band gap nature of the composite was observed, therefore, $n = 1/2$ was used for all the compositions. The value of band gap energy decreases from the CFA-BFA blend to 10% Mo@LOS-Z due to the increasing Mo loading [72]. This indicates the shifting of the absorption edge while increasing the interfacial charge transfer as the photons will require less energy to generate EHP for enhanced photocatalytic performance [73]. The highest band gap of the CFA-BFA blend in Figure 4.4(a) corresponds to the higher recombination rate which is evident from PL spectra therefore more energy is required to generate EHP for the photocatalytic activity. Similarly, LOS-Z in Figure 4.4(b) has a slightly lower band gap than the CFA-BFA blend however the recombination rate is still higher. In Figure 4.4(c-d), the narrowing in band gap was observed specifically for 10% Mo@LOS-Z (Figure 4.4(d)), indicating better photon absorption in the visible region and suppressing the EHP recombination effect.

Table 4.1: Band gap of the CFA-BFA blend, LOS-Z, 5% Mo@LOS-Z and 10% Mo@LOS-Z samples

Photocatalysts	Band Gap (eV)
CFA + BFA blend	3.37
LOS-Z	3.3
5% Mo@LOS-Z	3.24
10% Mo@LOS-Z	3.15

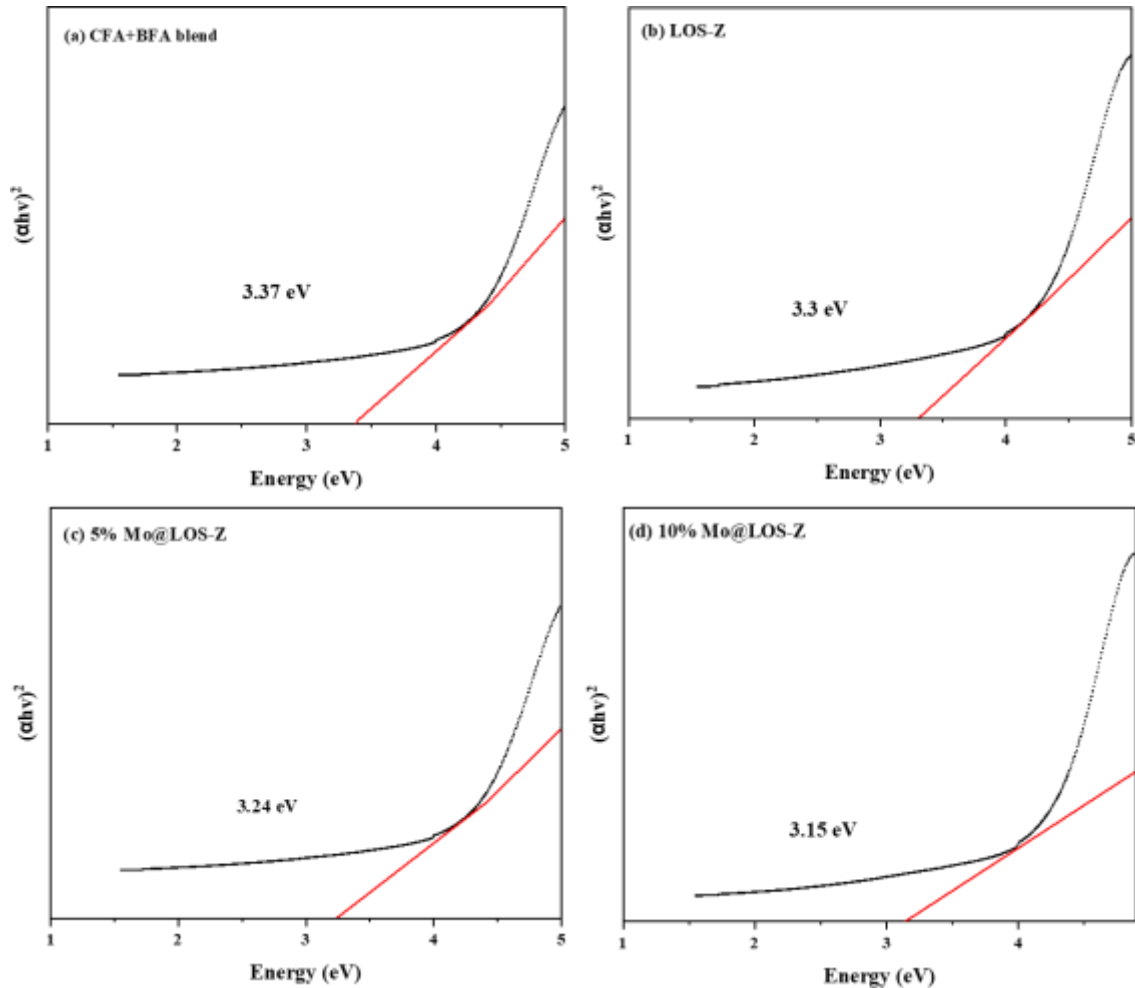


Figure 4.4: The band gap of (a) CFA-BFA blend, (b) LOS-Z, (c) 5% Mo@LOS-Z, and (d) 10% Mo@LOS-Z

The photocatalytic dye degradation efficiency of the CFA-BFA blend, LOS-Z, 5% Mo@LOS-Z and 10% Mo@LOS-Z samples are shown in [Figure 4.5\(a-d\)](#). The degradation efficiency demonstrates the order of samples as follows: 10% Mo@LOS-Z (82%) > 5% Mo@LOS-Z (77%) > LOS-Z (65%) > CFA-BFA blend (56%). The photocatalytic activity is enhanced due to the increase in Mo concentration, lower recombination effect and band gap. The reactive sites are increased by increasing the amount of Mo while lowering the band gap broadening the range of light and helping in the generation of charge carriers [74]. The experiments were repeated two times with an error below 5% to confirm the reproducibility of dye degradation for each sample. Moreover, when the Mo loading exceeded 10%, a significant decline in the properties and performance was observed and thus, photocatalyst with higher Mo concentration (15%) is not studied and reported in this study. The high instability and agglomeration decrease the catalytic performance as a result of excess Mo deposition on the surface of LOS-Z which can reduce the effective area for absorbing visible light in the LOS-Z matrix [75]. Therefore, different parametric studies of 10% Mo@LOS-Z were performed using different catalyst dosages (0.5 mg mL⁻¹ and 1 mg mL⁻¹) and MB concentrations (2.5 ppm and 7.5 ppm).

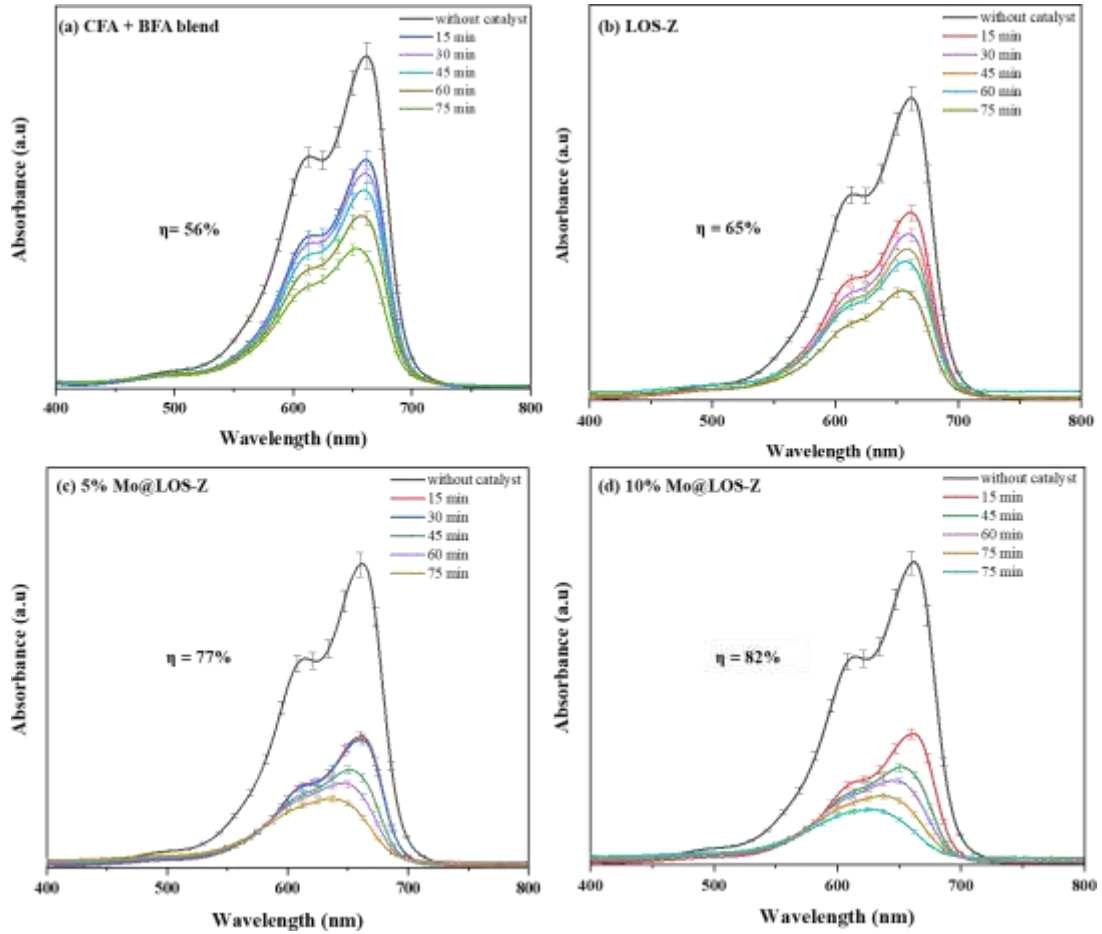


Figure 4.5: Photocatalytic dye degradation of MB using (a) CFA-BFA blend, (b) LOS-Z, (c) 5% Mo@LOS-Z, and (d) 10% Mo@LOS-Z

The pseudo-first-order kinetics was used to study the photodegradation experiments depending on the catalyst and MB degradation concentration. Eq. 11 describes the time dependence of MB decomposition using first-order kinetics.

$$\frac{dC}{dT} = k(C_0 - C) \quad (11)$$

Where C , C_0 and k show the MB concentration, initial MB concentration and rate constant respectively. Figure 4.6 presents the pseudo-first-order kinetics and the time vs C/C_0 (the order of reaction) whereas Table 4.2 shows the rate constants k and R^2 of MB. Figure 4.6(a)

shows the dye degradation over time while the degradation rate constants are calculated in Figure 4.6(b) using Eq. 11 which are found to be $7.02 \times 10^{-3} \text{ min}^{-1}$, $1.117 \times 10^{-2} \text{ min}^{-1}$, $1.785 \times 10^{-2} \text{ min}^{-1}$, and $2.09 \times 10^{-2} \text{ min}^{-1}$ for CFA-BFA blend, LOS-Z, 5% Mo@LOS-Z, and 10% Mo@LOS-Z samples respectively. The 10% Mo@LOS-Z sample showed better photocatalytic activity ($2.09 \times 10^{-2} \text{ min}^{-1}$) while lower activity was observed for the CFA-BFA blend sample. The decreasing trend is justified by the rate of creation of holes and conduction bands. As described in Table 4.2, the higher recombination of electrons and holes lowers the degradation rate, and very low visible light is absorbed by photons to degrade MB dye. Additionally, the band gap shift to the visible region caused the increase in photocatalytic activity with the increase in the concentration and mid-band formation. The dopants' mid-band within the band gap enables the broader light spectrum to be absorbed and as a result, more photons were absorbed from visible light illumination. A similar study was also reported for Mo-doped anatase photocatalytic activity [76]. This resulted in the improvement of 82% photocatalytic dye degradation.

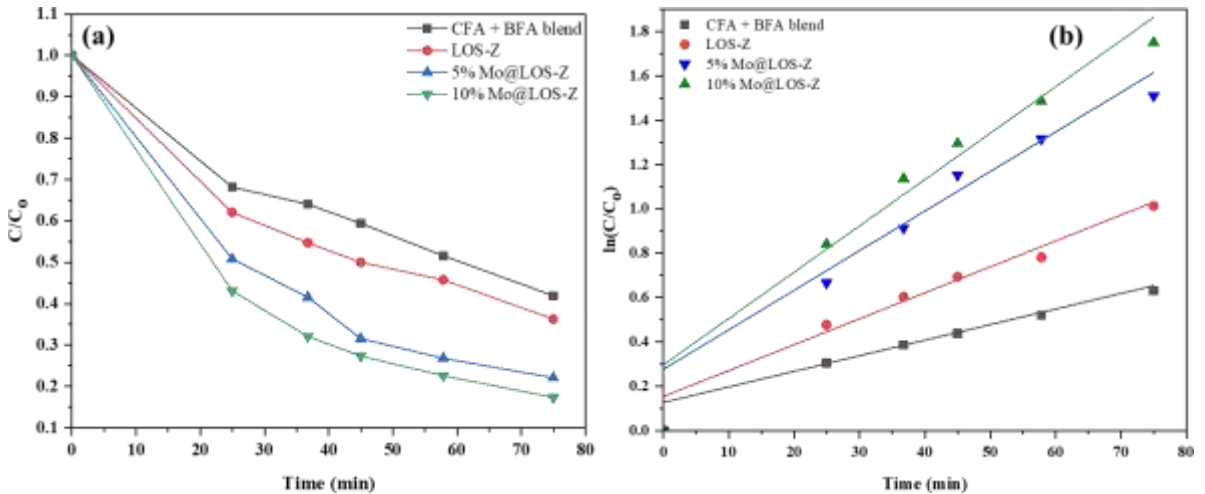


Figure 4.6: (a) photocatalytic degradation vs irradiation time, (b) pseudo-first-order kinetics of synthesized samples

Table 4.2: Rate constant (k) and R^2 of the CFA-BFA blend, LOS-Z, 5% Mo@LOS-Z, and 10% Mo@LOS-Z samples

Photocatalysts	k [min^{-1}]	R^2
CFA-BFA blend	7.02×10^{-3}	0.835
LOS-Z	1.117×10^{-2}	0.903
5% Mo@LOS-Z	1.785×10^{-2}	0.877
10% Mo@LOS-Z	2.09×10^{-2}	0.897

Based on the dye degradation efficiency and kinetic studies, the 10% Mo@LOS-Z shows the best results. Therefore, parametric studies were performed to justify the optimum catalyst dosage and MB concentration as these are the important parameters that play a significant role in the detailed study of various catalysts in dye degradation.

Figure 4.7(a-c) shows the degradation results for 0.5 mg mL^{-1} , 1 mg mL^{-1} , and 2 mg mL^{-1} 10% Mo@LOS-Z respectively while Figure 4.7(d) illustrates the best degradation result for 2 mg mL^{-1} catalyst therefore it is taken as the best catalyst dosage to be studied further for dye degradation experiments. This can be attributed to insufficient active sites that restrict MB adsorption at lower doses (0.5 mg mL^{-1} and 1 mg mL^{-1}), which drops degradation efficiency. For optimum photocatalytic efficiency, a dose of 2 mg mL^{-1} maximizes active site availability without aggregating or obstructing light penetration [77].

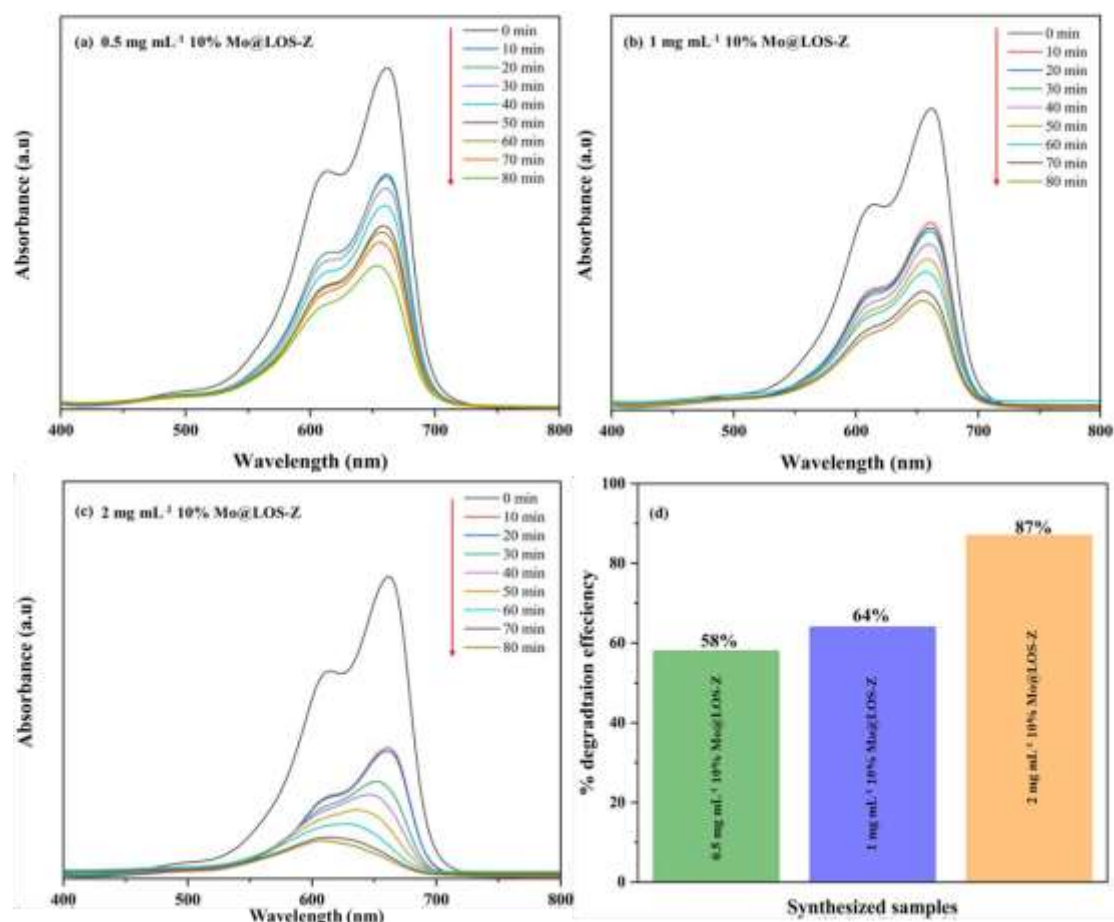


Figure 4.7: Catalyst dosage of (a) 0.5 mg mL⁻¹, (b) 1 mg mL⁻¹, (c) 2 mg mL⁻¹, and (d) % degradation efficiency of 10% Mo@LOS-Z in MB dye

Moreover, the experiments were also conducted by varying MB concentrations using the 2 mg mL⁻¹ catalyst dosage shown in Figure 4.8. It illustrates a significant change when MB concentration is varied. Figure 4.8(a-b) shows 13.98% and 65.7% degradation efficiency for 2.5 ppm and 7.5 ppm MB concentration respectively while 82% degradation efficiency was shown by 5 ppm MB solution (Figure 4.7(d)). At 2.5 ppm MB concentration, the restricted availability and low concentration of MB molecules enable low interaction with the catalyst's active sites, which results in low degradation efficiency [78]. Conversely, a 7.5 ppm dye solution which is highly concentrated can limit the amount

of light entering the system and hinder photon penetration which is required for the photodegradation process [79]. To optimize light penetration, produce reactive species effectively and attain the optimum degradation efficiency, the ideal concentration of 5 ppm shows a balance between the MB molecules that interact with the catalyst efficiently. Thus, it can be considered a suitable concentration for further studies.

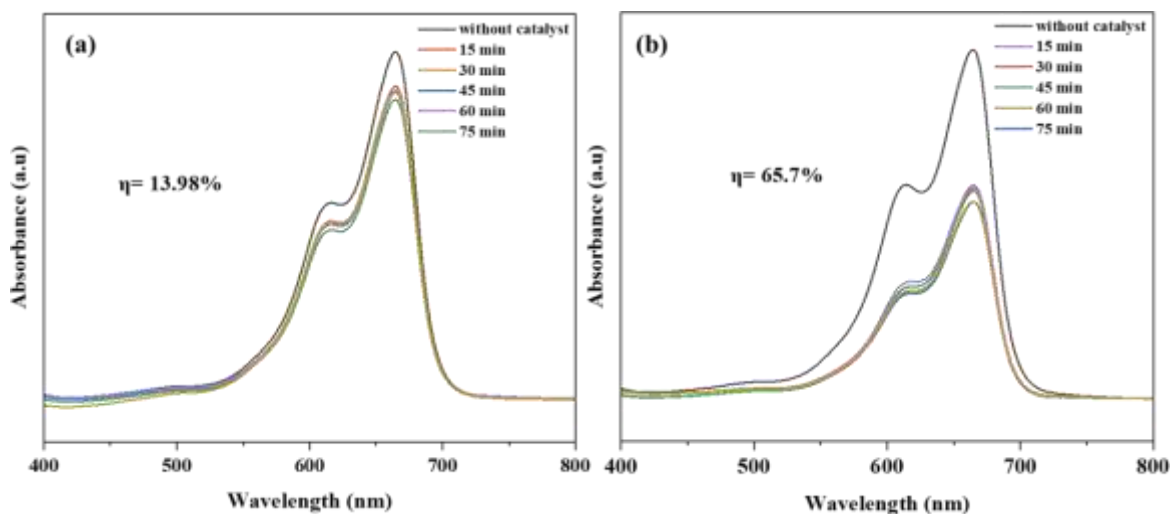


Figure 4.8: Varying MB concentration (a) 2.5 ppm and (b) 7.5 ppm using 2 mg mL^{-1} catalyst dose

To study the reusability of the photocatalyst, dye degradation was investigated using 2 mg mL^{-1} used 10% Mo@LOS-Z catalyst in 5 ppm MB concentration. The result in [Figure 4.9](#) shows that the photocatalyst lost its efficiency from 82% to 43.38%. The degradation performance drop was due to the sedimentation of MB dye across the repeated run. Moreover, contaminants are absorbed on the photocatalyst surface and the number of active sites that are already utilized in the first degradation pathway are reduced or blocked therefore very few photons are accessible to reach the surface of the photocatalyst. This resulted in less $\cdot\text{OH}$ formation and thus a lesser amount of percentage degradation [80].

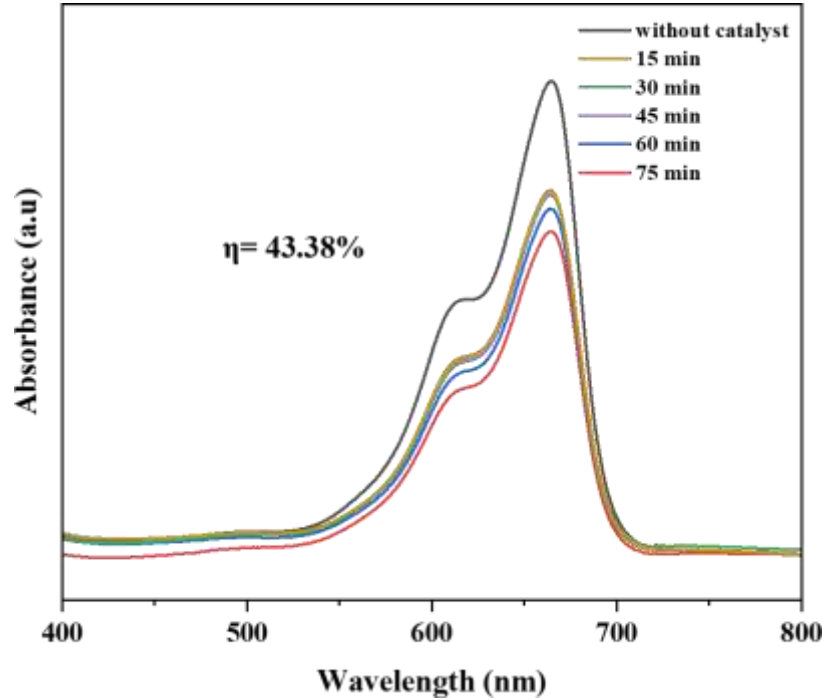


Figure 4.9: Reusability of 10% Mo@LOS-Z photocatalyst

4.3 Photocatalytic reaction mechanism for dye degradation

Photocatalytic dye degradation happens when electrons from the valence band (VB) are transferred to the conduction band (CB). The photocatalyst absorbs photons from sunlight or a lamp. This is responsible for the accumulation of CB electrons (e^-) and the VB holes (h^+) which further initiate chemical reactions. It is important to consider the recombination rate of the EHP as the e^- from CB suddenly returns to VB providing time of reaction only with the adsorbed molecules [81]. This consideration is affected by the choice of both photocatalyst and lamp.

In the case of dye degradation, the electrons are converted into superoxide radicals by reacting with dissolved oxygen molecules present on the surface of the catalyst. Some of the electrons, having no time for a reaction with oxygen, recombine back with adsorbed

molecules such as MB. Therefore, oxygen molecules are actively responsible for photocatalytic dye degradation [82]. For a deeper analysis of the photocatalytic dye degradation mechanism of 10% Mo@LOS-Z, a radical trap test was conducted to observe the dominant effect of active species. Ascorbic acid, IPA, EDTA, and cupric nitrate were added to the solution as superoxide radicals ($^{\bullet}\text{O}_2^-$), hydroxyl radicals ($^{\bullet}\text{OH}$), holes (H^+), and electrons (e^-) respectively. Figure 4.10, shows that the photocatalytic activity decreased significantly when IPA was added, revealing ($^{\bullet}\text{OH}$) as a major contributor to the process of photocatalytic process. This lowers the concentration and hinders the efficiency. Furthermore, the results also indicate the influence of active species in the MB decomposition with the order of $^{\bullet}\text{OH} > \text{e}^- > \text{H}^+ > ^{\bullet}\text{O}_2^-$.

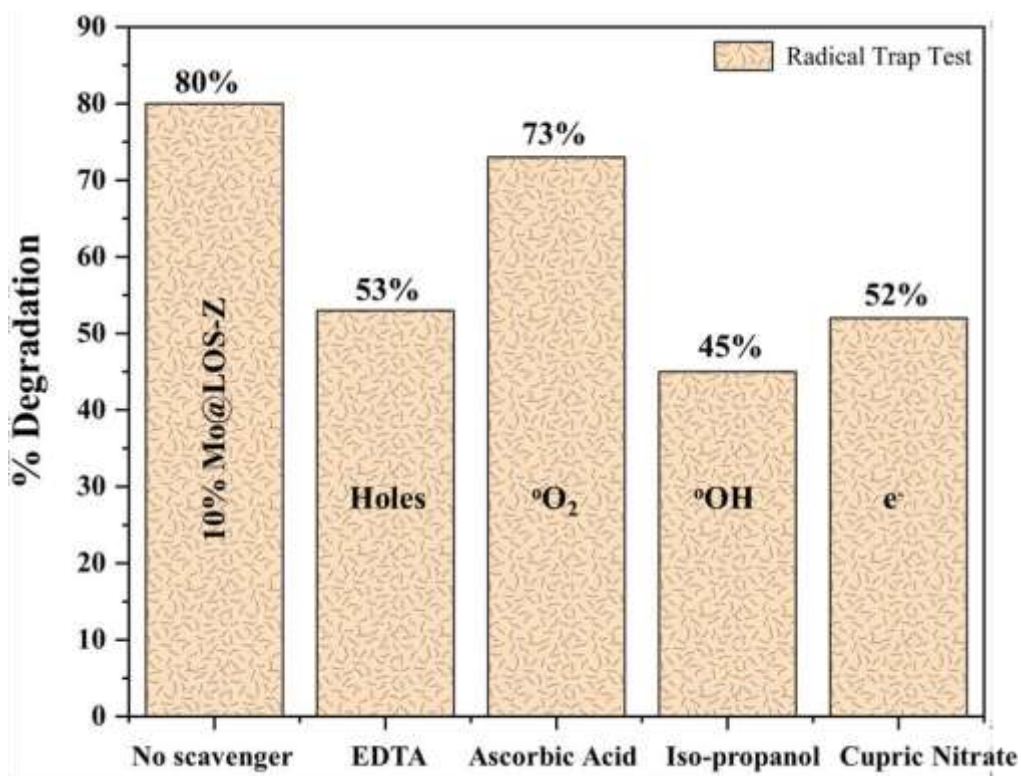
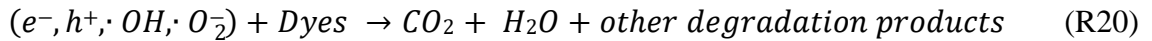
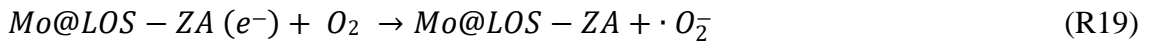
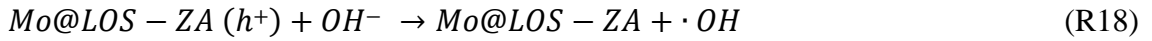
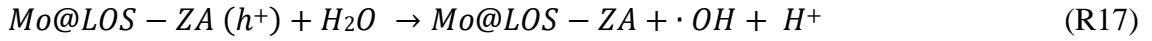
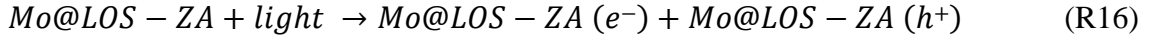


Figure 4.10: Active radical trap test of 10% Mo@LOS-Z

A possible mechanism of MB dye photocatalytic degradation is proposed in the following chemical equation (R (16) – (20)) and presented in Figure 4.11.



10% Mo@LOS-Z significantly broadened the photo response range of the 10% Mo@LOS-Z composite. When the light is irradiated, the transition of electrons occurs from the VB of 10% Mo@LOS-Z to the CB due to the successful generation of EHP. This caused oxidation and degradation of adsorbed MB by photo-induced holes. As a result, the electrons present on CB reduced dissolved oxygen to superoxide radicals ($\cdot O_2^-$) and the holes present in VB produce hydroxyl radicals ($\cdot OH$). Therefore, MB is degraded due to the predominant effect of ($\cdot OH$) and ($\cdot O_2^-$) radicals.

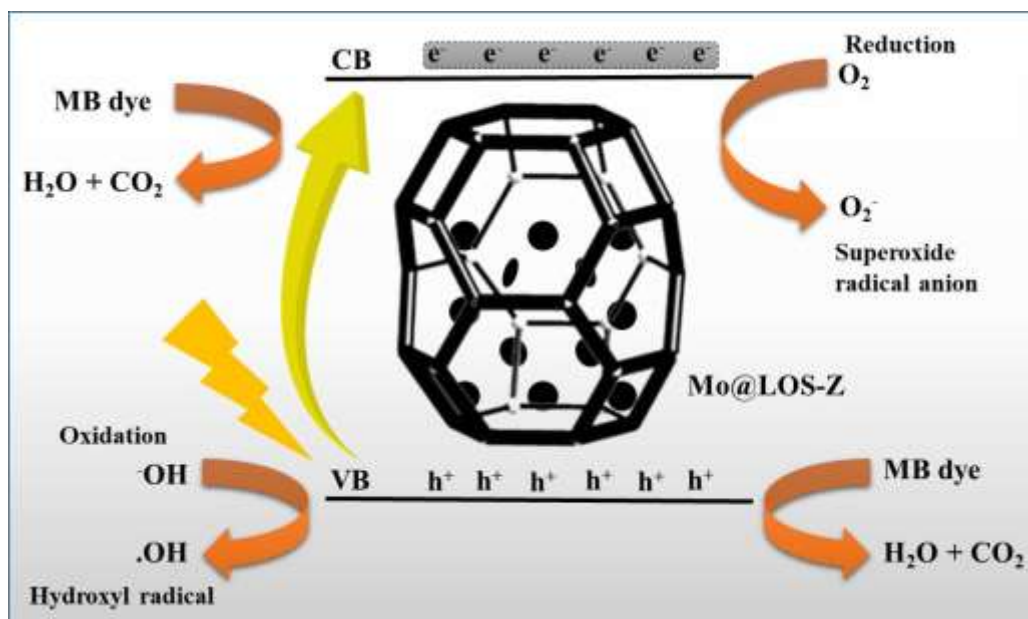


Figure 4.11: Photodegradation mechanism of MB using 10% Mo@LOS-Z photocatalyst under visible lamp

The degradation performance of various photocatalysts under different light sources and pollutants is discussed in [Table 4.3](#). Under a 35 W Xe lamp, the present study shows 82% degradation efficiency of MB and overall enhanced performance of 10% Mo@LOS-Z. However, this is less than some other catalysts reported in the literature that achieved 100% degradation of MB with strong light sources, such as RGO/TiO₂/Zeolite4A and bayerite/zeolite-TiO₂ but comparable performance can be observed by Ag@CdSe/Zeolite and Zeolite-ZnO. Thus, by adjusting light sources or catalyst modifications, degradation rates can potentially be improved further.

The degradation performances of similar photocatalysts is presented in [Table 4.3](#).

Table 4.3: Comparison of different studies of photocatalytic dye degradation

Photocatalysts	Light sources	Pollutants	Degradation efficiency	Ref.
10% Mo@LOS-Z	35 W Xe lamp	MB	82%	This work
RGO/TiO ₂ /Zeolite4A	125 W Hg vapour lamp	MB	100%	[83]
Bayerite/zeolite-TiO ₂	300 W Xe lamp	MB	100%	[84]
TiO ₂ /Zeolite4A	125 W Hg vapour lamp	MB	-	[85]
Zeolite/g-C ₃ N ₄ /ZnO/CeO ₂	85 W incandescent bulb	MB	95.89%	[86]
Ag@CdSe/Zeolite	300 W tungsten-halogen lamp	MB	89.98%	[87]
Zeolite-ZnO	35 W Xe lamp	RhB	81%	[88]
Zeolite-supported nano-zerovalent iron	-	AO52	80%	[89]

4.4 Photocatalytic hydrogen evolution

CFA-BFA blend, LOS-Z, 5% Mo@LOS-Z, and 10% Mo@LOS-Z were used for photocatalytic H₂ production from the dye-degraded water and methanol as a scavenger to comparatively analyze their performance. It is shown in Figure 4.12.

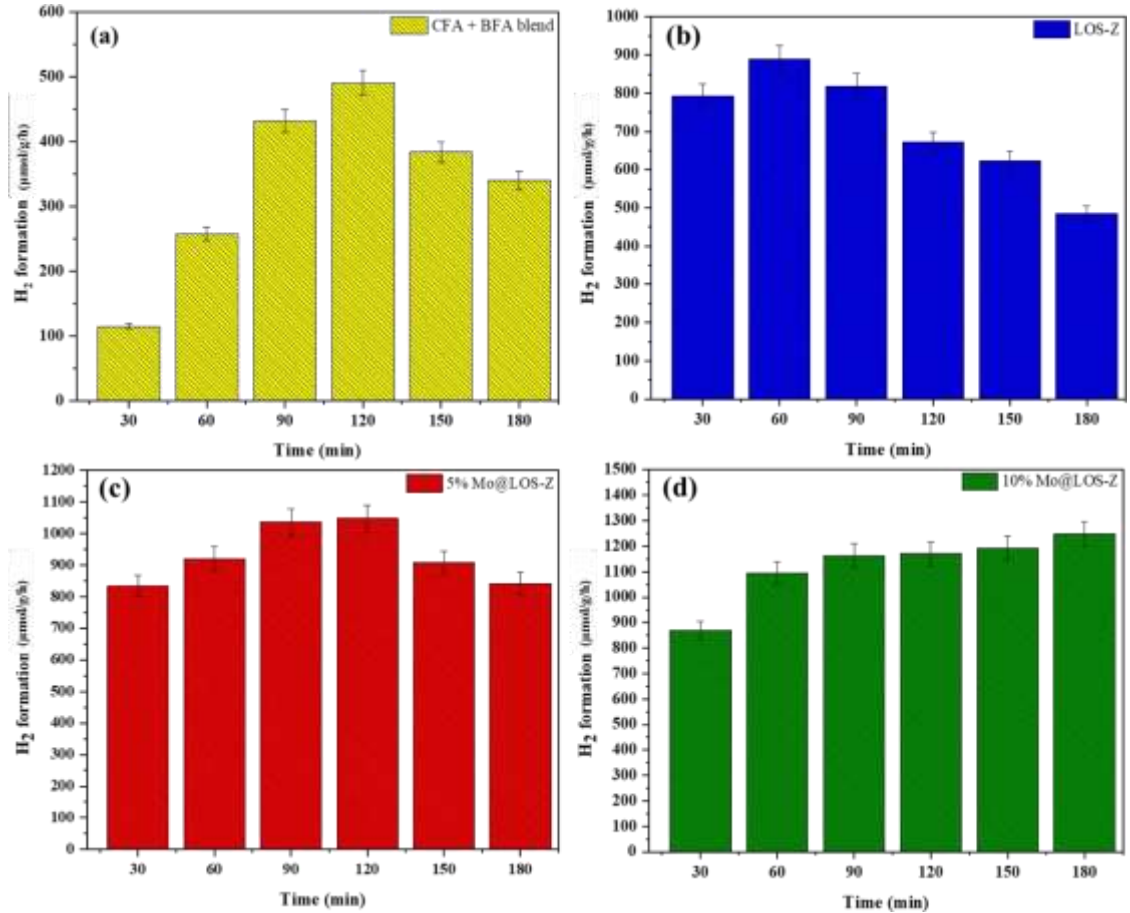
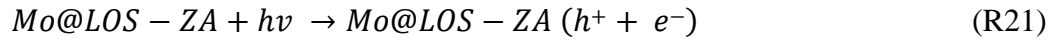


Figure 4.12: H₂ production of treated dye water during photocatalytic oxidation of methanol in the presence of (a) CFA-BFA blend, (b) LOS-Z, (c) 5% Mo@LOS-Z, and (d) 10% Mo@LOS-Z photocatalyst

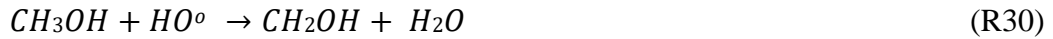
Figure 4.12(a) shows the initial increase in H₂ production ($\sim 480 \mu\text{mol g}^{-1}\text{h}^{-1}$) for the CFA-BFA blend in the first 120 min followed by a drop due to its large band gap (3.37 eV) and high recombination rates. The LOS-Z in Figure 4.12(b) shows a rapid increase in H₂ production ($\sim 890 \mu\text{mol g}^{-1}\text{h}^{-1}$) in 60 min and a drop ($\sim 500 \mu\text{mol g}^{-1}\text{h}^{-1}$) in 180 min

indicating improved structural and catalytic properties after synthesis. In [Figure 4.12\(c\)](#), the 5% Mo@LOS-Z remains stable between 90-120 min proving mid-gap state formation for a certain period. The production of H₂ reaches up to ~1000 μmol g⁻¹h⁻¹, which decreases to ~800 μmol g⁻¹h⁻¹ due to the saturation of mid-gap states with charge carriers after a prolonged reaction time. [Figure 4.12\(d\)](#) shows an increasing trend for 10% Mo@LOS-Z and the highest H₂ production (~1200 μmol g⁻¹h⁻¹) among all the samples. This photocatalyst has the lowest band gap (3.15 eV) for visible light absorption and reduced recombination rates making it the most efficient photocatalyst for H₂ production. The experiments were repeated two times with an error below 5% to confirm the reproducibility of H₂ production for each sample.

A similar reaction pathway of methanol oxidation including side reactions is described by Oros-Ruis et al. [91] as follows ([R21-R27](#)):



It is evident from R23 that the rapid increase in hydrogen evolution is because of photogenerated electrons used for H⁺ reduction. Furthermore, the hydrogen produced from methanol oxidation is described in (R28-33) [107].



The production of H₂ by the oxidation of methanol is proposed in the reaction mechanism. The reaction is initiated by Mo@LOS-Z excitation when light falls and forms an EHP pair. The holes oxidized water to oxygen and hydrogen ions while the electrons reduced hydrogen ions to H₂. Methanol favoured the direct oxidation of h⁺ thus forming hydrogen ions and aldehydes. Further, the methanol oxidation proceeded to H₂ and aldehydes.

The suppression of recombination effect is an important factor of a good photocatalyst. By preparing a composite, the electronic properties influenced the photogenerated electrons and holes separation, reducing the charge recombination probability as discussed in PL spectra. Moreover, the change in band gap energy was also observed for 10% Mo@LOS-Z extending the lifetime of photogenerated EHPs, increasing

photocatalytic activity. The mechanism of photocatalysis of H₂ production is illustrated in the Figure 4.13.

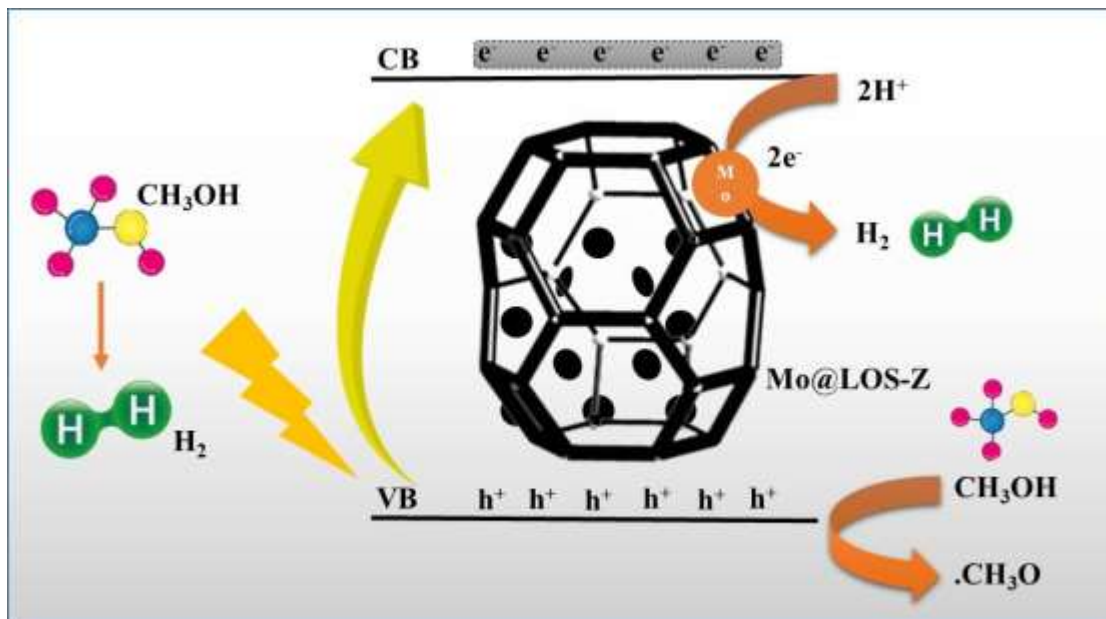


Figure 4.13: Photodegradation mechanism of H₂ using 10% Mo@LOS-Z photocatalyst under Xe lamp

Table 4.4 presents the performance of similar photocatalysts in H₂ production using various light sources. 10% Mo@LOS-Z outperformed many other catalysts and can be considered an economical and sustainable alternative, showing an H₂ production rate of 1200 μmol g⁻¹h⁻¹ under a 35 W Xe lamp except ZeoNa-Y@TiO₂/Pd which shows a maximum H₂ production rate of 3.5 mmol g⁻¹h⁻¹.

Table 4.4: Comparison of different catalysts used in photocatalytic H₂ production

Photocatalysts	Light sources	H₂ production rate	References
10% Mo@LOS-Z	35 W Xe lamp	1200 $\mu\text{mol g}^{-1}\text{h}^{-1}$	This work
Zeolite LTA/TiO ₂	300 W Xe lamp	238.3 $\mu\text{mol g}^{-1}\text{h}^{-1}$	[32]
ZnO/ZnS-3h-NiS	300 W Osram Vita Lux lamp	26 $\mu\text{mol g}^{-1}\text{h}^{-1}$	[93]
ZeoNa-Y@TiO ₂ /Pd	400W Xe lamp	3.5 mmol $\text{g}^{-1}\text{h}^{-1}$	[94]
0.2 wt% Nd/TiO ₂	150 W Xe lamp	300 $\mu\text{mol g}^{-1}\text{h}^{-1}$	[92]

Chapter 5: Conclusions and Future Recommendation

5.1 Conclusions

This study presents the synthesis of LOS-Z from the waste-derived CFA-BFA blend. The impregnation of Mo in the LOS-Z matrix enhanced the absorption of visible light, improved charge transfer and resisted the charge combination by shifting the spectrum towards the visible range, narrowing the band gap and recombination rate respectively. The XRD and FTIR confirmed the synthesis of catalysts while optoelectronic properties reveal successful engineering of band gap and recombination effect. The 10% Mo@LOS-Z narrowed the band gap to 3.15 eV which falls in the visible region. This claim is proven by the photocatalytic experiments showing 10% Mo@LOS-Z exhibits better performance in degrading MB dye ($\eta = 82\%$) and H₂ production ($\sim 1200 \mu\text{mol g}^{-1}\text{h}^{-1}$). This catalytic performance is competitive with and in certain situations better than other catalysts using expensive and rare metals. Thus, it can be a viable option for photocatalytic H₂ production owing to its high efficiency and sustainability as a waste-derived material which makes it an advantageous option for future energy applications. However, for a more thorough understanding, future studies can benefit from advanced characterizations and computational studies for more atomistic insights.

5.2 Recommendations

In this work, a photocatalyst was synthesized using blends of coal and biomass fly ash been prepared via hydrothermal method, and then Mo incorporated into the synthesized material to boost its activity. Material properties of the developed composites were

characterized using various techniques. However, to examine these properties more effectively, some other factors can be adjusted including the temperature, the amount of photocatalyst loaded onto the substrate, the sacrificial reagents such as methanol, ethanol, isopropanol, etc., the light source whether LED or the power of xenon lamp, and the type of electrolyte such as freshwater, seawater, sludge, or degraded dye solution. All these parameters can impact the performance of photocatalysts, but we set up the best of the parameters as we had observed in our literature review due to time constraints and resource limitations.

REFERENCES

- [1] O. Edenhofer, R. Pichs-Madruga, Y. Sokona, K. Seyboth, S. Kadner, T. Zwickel, P. Eickemeier, G. Hansen, S. Schlömer, C. von Stechow, Renewable energy sources and climate change mitigation: Special report of the intergovernmental panel on climate change, Cambridge University Press 2011.
- [2] S. San Martín, M.J. Rivero, I. Ortiz, Unravelling the mechanisms that drive the performance of photocatalytic hydrogen production, *Catalysts*, 10 (2020) 901.
- [3] E. Pastor, M. Sachs, S. Selim, J.R. Durrant, A.A. Bakulin, A. Walsh, Electronic defects in metal oxide photocatalysts, *Nature Reviews Materials*, 7 (2022) 503-521.
- [4] G. Hu, J. Yang, X. Duan, R. Farnood, C. Yang, J. Yang, W. Liu, Q. Liu, Recent developments and challenges in zeolite-based composite photocatalysts for environmental applications, *Chemical Engineering Journal*, 417 (2021) 129209.
- [5] J. Liu, Y. Wang, Z. Dai, C.Q. Jia, L. Yang, J. Liu, Y. Chen, L. Yao, B. Wang, W. Huang, Recent advances in Zeolite-based catalysts for volatile organic compounds decontamination by thermal catalytic oxidation, *Separation and Purification Technology*, (2023) 125339.
- [6] Z. Wu, Y. Su, J. Yu, W. Xiao, L. Sun, C. Lin, Enhanced photoelectrocatalytic hydrogen production activity of SrTiO₃-TiO₂ hetero-nanoparticle modified TiO₂ nanotube arrays, *International journal of hydrogen energy*, 40 (2015) 9704-9712.
- [7] W. Zhao, Z. Chen, X. Yang, X. Qian, C. Liu, D. Zhou, T. Sun, M. Zhang, G. Wei, P.D. Dissanayake, Recent advances in photocatalytic hydrogen evolution with high-performance catalysts without precious metals, *Renewable and Sustainable Energy Reviews*, 132 (2020) 110040.
- [8] B. Tamilarasi, K. Jithul, J. Pandey, Non-noble metal-based electro-catalyst for the oxygen evolution reaction (OER): Towards an active & stable electro-catalyst for PEM water electrolysis, *International Journal of Hydrogen Energy*, 58 (2024) 556-582.
- [9] P. Chandra, A. Mohammad, B. Tripathi, T. Yoon, Recent advancements in molybdenum disulfide (MoS₂) and its functional nanostructures for photocatalytic and non-photocatalytic organic transformations, *Flatchem*, 34 (2022) 100395.
- [10] A. Iqbal, H. Sattar, R. Haider, S. Munir, Synthesis and characterization of pure phase zeolite 4A from coal fly ash, *Journal of Cleaner Production*, 219 (2019) 258-267.
- [11] C. Acar, I. Dincer, G.F. Naterer, Review of photocatalytic water-splitting methods for sustainable hydrogen production, *International Journal of Energy Research*, 40 (2016) 1449-1473.

- [12] K.O. Yoro, M.O. Daramola, CO₂ emission sources, greenhouse gases, and the global warming effect, *Advances in carbon capture*, Elsevier2020, pp. 3-28.
- [13] C.G. Scanes, Human activity and habitat loss: destruction, fragmentation, and degradation, *Animals and human society*, Elsevier2018, pp. 451-482.
- [14] F. Qureshi, M. Yusuf, M.A. Khan, H. Ibrahim, B.C. Ekeoma, H. Kamyab, M.M. Rahman, A.K. Nadda, S. Chelliapan, A State-of-The-Art Review on the Latest trends in Hydrogen production, storage, and transportation techniques, *Fuel*, 340 (2023) 127574.
- [15] M. Shah, P. Mondal, A.K. Nayak, A. Bordoloi, Hydrogen from natural gas, *Sustainable utilization of natural resources*, CRC Press2017, pp. 81-120.
- [16] L. Barelli, G. Bidini, F. Gallorini, S. Servili, Hydrogen production through sorption-enhanced steam methane reforming and membrane technology: a review, *Energy*, 33 (2008) 554-570.
- [17] S.M. Soltani, A. Lahiri, H. Bahzad, P. Clough, M. Gorbounov, Y. Yan, Sorption-enhanced steam methane reforming for combined CO₂ capture and hydrogen production: a state-of-the-art review, *Carbon Capture Science & Technology*, 1 (2021) 100003.
- [18] M. Amin, H.H. Shah, A.G. Fareed, W.U. Khan, E. Chung, A. Zia, Z.U.R. Farooqi, C. Lee, Hydrogen production through renewable and non-renewable energy processes and their impact on climate change, *International journal of hydrogen energy*, 47 (2022) 33112-33134.
- [19] J.-R. Han, S.-J. Park, H. Kim, S. Lee, J.M. Lee, Centralized and distributed hydrogen production using steam reforming: challenges and perspectives, *Sustainable Energy & Fuels*, 6 (2022) 1923-1939.
- [20] M. Rashid, M.K. Al Mesfer, H. Naseem, M. Danish, Hydrogen production by water electrolysis: a review of alkaline water electrolysis, PEM water electrolysis and high temperature water electrolysis, *International Journal of Engineering and Advanced Technology*, (2015).
- [21] M.A. Laguna-Bercero, Recent advances in high temperature electrolysis using solid oxide fuel cells: A review, *Journal of Power sources*, 203 (2012) 4-16.
- [22] J. Chi, H. Yu, Water electrolysis based on renewable energy for hydrogen production, *Chinese Journal of Catalysis*, 39 (2018) 390-394.
- [23] R. Chaubey, S. Sahu, O.O. James, S. Maity, A review on development of industrial processes and emerging techniques for production of hydrogen from renewable and sustainable sources, *Renewable and Sustainable Energy Reviews*, 23 (2013) 443-462.
- [24] X. Xu, Q. Zhou, D. Yu, The future of hydrogen energy: Bio-hydrogen production technology, *International Journal of Hydrogen Energy*, 47 (2022) 33677-33698.

- [25] G. Balachandar, N. Khanna, D. Das, Biohydrogen production from organic wastes by dark fermentation, *Biohydrogen*, Elsevier2013, pp. 103-144.
- [26] C. Putatunda, M. Behl, P. Solanki, S. Sharma, S.K. Bhatia, A. Walia, R.K. Bhatia, Current challenges and future technology in photofermentation-driven biohydrogen production by utilizing algae and bacteria, *International Journal of Hydrogen Energy*, 48 (2023) 21088-21109.
- [27] R. Moore, E. Parma, B. Russ, W. Sweet, M. Helie, N. Pons, P. Pickard, An integrated laboratory-scale experiment on the sulfur-iodine thermochemical cycle for hydrogen production, *High Temperature Reactor Technology*, 2008, pp. 541-549.
- [28] X. Vitart, A. Le Duigou, P. Carles, Hydrogen production using the sulfur-iodine cycle coupled to a VHTR: an overview, *Energy conversion and management*, 47 (2006) 2740-2747.
- [29] T.K. Tulu, S.M. At naw, R.D. Bededa, D.G. Wakshume, V.R. Ancha, Kinetic modeling and optimization of biomass gasification in bubbling fluidized bed gasifier using response surface method, *Int J Renew Energy Dev*, 11 (2022).
- [30] K. Kalyanasundaram, *Photochemical applications of solar energy: photocatalysis and photodecomposition of water*, (2013).
- [31] S. Protti, A. Albin, N. Serpone, Photocatalytic generation of solar fuels from the reduction of H₂O and CO₂: a look at the patent literature, *Physical Chemistry Chemical Physics*, 16 (2014) 19790-19827.
- [32] M. Dehghanimadvar, R. Shirmohammadi, M. Sadeghzadeh, A. Aslani, R. Ghasempour, Hydrogen production technologies: attractiveness and future perspective, *International Journal of Energy Research*, 44 (2020) 8233-8254.
- [33] A.M. Abdalla, S. Hossain, O.B. Nisfindy, A.T. Azad, M. Dawood, A.K. Azad, Hydrogen production, storage, transportation and key challenges with applications: A review, *Energy conversion and management*, 165 (2018) 602-627.
- [34] A.S. Qureshi, Challenges and prospects of using treated wastewater to manage water scarcity crises in the Gulf Cooperation Council (GCC) countries, *Water*, 12 (2020) 1971.
- [35] D. Zhu, Q. Zhou, Action and mechanism of semiconductor photocatalysis on degradation of organic pollutants in water treatment: A review, *Environmental Nanotechnology, Monitoring & Management*, 12 (2019) 100255.
- [36] S.H. Khan, B. Pathak, Zinc oxide based photocatalytic degradation of persistent pesticides: A comprehensive review, *Environmental nanotechnology, monitoring & management*, 13 (2020) 100290.

- [37] M. Ashraf, M. Ayaz, M. Khan, S.F. Adil, W. Farooq, N. Ullah, M. Nawaz Tahir, Recent trends in sustainable solar energy conversion technologies: mechanisms, prospects, and challenges, *Energy & Fuels*, 37 (2023) 6283-6301.
- [38] A. Singh, N. Sharma, Photocatalytic Hydrogen Production for Green Energy, *Materials Chemistry and Physics*, (2024) 129342.
- [39] K. Hashimoto, H. Irie, A. Fujishima, TiO₂ photocatalysis: a historical overview and future prospects, *Japanese journal of applied physics*, 44 (2005) 8269.
- [40] M. Sohail, S. Rauf, M. Irfan, A. Hayat, M.M. Alghamdi, A.A. El-Zahhar, D. Ghernaout, Y. Al-Hadeethi, W. Lv, Recent developments, advances and strategies in heterogeneous photocatalysts for water splitting, *Nanoscale advances*, 6 (2024) 1286-1330.
- [41] Y. Zhang, Y.-J. Heo, J.-W. Lee, J.-H. Lee, J. Bajgai, K.-J. Lee, S.-J. Park, Photocatalytic hydrogen evolution via water splitting: A short review, *Catalysts*, 8 (2018) 655.
- [42] A.O. Ibadon, P. Fitzpatrick, Heterogeneous photocatalysis: recent advances and applications, *Catalysts*, 3 (2013) 189-218.
- [43] Z. Mamiyev, N.O. Balayeva, Metal sulfide photocatalysts for hydrogen generation: A review of recent advances, *Catalysts*, 12 (2022) 1316.
- [44] A.K. Singh, R.E. Masto, B. Hazra, J. Esterle, P.K. Singh, A.K. Singh, R.E. Masto, B. Hazra, J. Esterle, P.K. Singh, Utilization of coal and biomass ash, *Ash from Coal and Biomass Combustion*, (2020) 37-89.
- [45] S.K. Upadhyay, S.A. Edrisi, Developing sustainable measures to restore fly-ash contaminated lands: Current challenges and future prospects, *Land Degradation & Development*, 32 (2021) 4817-4831.
- [46] G. Li, C. Zhou, W. Ahmad, K.I. Usanova, M. Karelina, A.M. Mohamed, R. Khallaf, Fly ash application as supplementary cementitious material: A review, *Materials*, 15 (2022) 2664.
- [47] H.-H.T. Nguyen, H.T. Nguyen, S.F. Ahmed, N. Rajamohan, M. Yusuf, A. Sharma, P. Arunkumar, B. Deepanraj, H.-T. Tran, A. Al-Gheethi, Emerging waste-to-wealth applications of fly ash for environmental remediation: A review, *Environmental research*, (2023) 115800.
- [48] T. Iqbal, C.-q. Dong, Q. Lu, Z. Ali, I. Khan, Z. Hussain, A. Abbas, Sketching Pakistan's energy dynamics: Prospects of biomass energy, *Journal of renewable and sustainable energy*, 10 (2018).
- [49] P. Kishor, A.K. Ghosh, D. Kumar, Use of fly ash in agriculture: A way to improve soil fertility and its productivity, *Asian Journal of Agricultural Research*, 4 (2010) 1-14.

- [50] L. Panda, S. Dash, Characterization and utilization of coal fly ash: a review, *Emerging Materials Research*, 9 (2020) 921-934.
- [51] A. Saraber, Fly ash from coal and biomass for use in concrete, Origin, properties and performance, (2017).
- [52] K. Shaila, D. Nisha, P. Pralhad, P. Deepa, Zeolite synthesis strategies from coal fly ash: a comprehensive review of literature, *International Research Journal in Environment Sciences*, 4 (2015) 93-99.
- [53] W. Chen, G. Song, Y. Lin, J. Qiao, T. Wu, X. Yi, S. Kawi, Synthesis and catalytic performance of Linde-type A zeolite (LTA) from coal fly ash utilizing microwave and ultrasound collaborative activation method, *Catalysis Today*, 397 (2022) 407-418.
- [54] C.S. Cundy, P.A. Cox, The hydrothermal synthesis of zeolites: history and development from the earliest days to the present time, *Chemical reviews*, 103 (2003) 663-702.
- [55] W. Sieber, W.M. Meier, Formation and properties of losod, a new sodium zeolite, *Helvetica Chimica Acta*, 57 (1974) 1533-1549.
- [56] J. Klinowski, J. Thomas, C. Fyfe, J.S. Hartman, Applications of magic-angle-spinning silicon-29 nuclear magnetic resonance. Evidence for two different kinds of silicon-aluminum ordering in zeolitic structures, *The Journal of Physical Chemistry*, 85 (1981) 2590-2594.
- [57] S.G. Kumar, K.K. Rao, Zinc oxide based photocatalysis: tailoring surface-bulk structure and related interfacial charge carrier dynamics for better environmental applications, *Rsc Advances*, 5 (2015) 3306-3351.
- [58] A. Zacco, L. Borgese, A. Gianoncelli, R.P. Struis, L.E. Depero, E. Bontempi, Review of fly ash inertisation treatments and recycling, *Environmental Chemistry Letters*, 12 (2014) 153-175.
- [59] C. Gao, F. Lyu, Y. Yin, Encapsulated metal nanoparticles for catalysis, *Chemical Reviews*, 121 (2020) 834-881.
- [60] A. Corma, H. Garcia, Zeolite-based photocatalysts, *Chemical communications*, (2004) 1443-1459.
- [61] H. Fatima, M.R. Azhar, Y. Zhong, Y. Arafat, M. Khiadani, Z. Shao, Rational design of ZnO-zeolite imidazole hybrid nanoparticles with reduced charge recombination for enhanced photocatalysis, *Journal of Colloid and Interface Science*, 614 (2022) 538-546.
- [62] V. Kumaravel, M.D. Imam, A. Badreldin, R.K. Chava, J.Y. Do, M. Kang, A. Abdel-Wahab, Photocatalytic hydrogen production: role of sacrificial reagents on the activity of oxide, carbon, and sulfide catalysts, *Catalysts*, 9 (2019) 276.

- [63] J. Corredor, M.J. Rivero, C.M. Rangel, F. Gloaguen, I. Ortiz, Comprehensive review and future perspectives on the photocatalytic hydrogen production, *Journal of Chemical Technology & Biotechnology*, 94 (2019) 3049-3063.
- [64] T. Salthammer, U. Hohm, M. Stahn, S. Grimme, Proton-transfer rate constants for the determination of organic indoor air pollutants by online mass spectrometry, *RSC advances*, 13 (2023) 17856-17868.
- [65] A. Elfasakhany, Investigations on the effects of ethanol–methanol–gasoline blends in a spark-ignition engine: performance and emissions analysis, *Engineering Science and Technology, an International Journal*, 18 (2015) 713-719.
- [66] C.R. López, E.P. Melián, J.O. Méndez, D.E. Santiago, J.D. Rodríguez, O.G. Díaz, Comparative study of alcohols as sacrificial agents in H₂ production by heterogeneous photocatalysis using Pt/TiO₂ catalysts, *Journal of Photochemistry and Photobiology A: Chemistry*, 312 (2015) 45-54.
- [67] H. Ahmad, S. Kamarudin, L.J. Minggu, M. Kassim, Hydrogen from photo-catalytic water splitting process: A review, *Renewable and Sustainable Energy Reviews*, 43 (2015) 599-610.
- [68] J. Li, Y. Liu, H. Li, C. Chen, Fabrication of g-C₃N₄/TiO₂ composite photocatalyst with extended absorption wavelength range and enhanced photocatalytic performance, *Journal of Photochemistry and Photobiology A: Chemistry*, 317 (2016) 151-160.
- [69] M. Kavehrad, Sustainable energy-efficient wireless applications using light, *IEEE Communications Magazine*, 48 (2010) 66-73.
- [70] M.T. Shabbir, T. Hussain, S. Shakir, M. Anwar, A.H. Khoja, S. Nawaz, A.N. Satti, Enhancement in the photocatalytic and optoelectronic properties of erbium oxide by adding zinc oxide and molybdenum, *Ceramics International*, 49 (2023) 19691-19700.
- [71] A. Mills, An overview of the methylene blue ISO test for assessing the activities of photocatalytic films, *Applied Catalysis B: Environmental*, 128 (2012) 144-149.
- [72] D.P. Jaihindh, C.-C. Chen, Y.-P. Fu, Reduced graphene oxide-supported Ag-loaded Fe-doped TiO₂ for the degradation mechanism of methylene blue and its electrochemical properties, *RSC advances*, 8 (2018) 6488-6501.
- [73] C. Jin, C. Ge, Z. Jian, Y. Wei, Facile synthesis and high photocatalytic degradation performance of ZnO-SnO₂ hollow spheres, *Nanoscale Research Letters*, 11 (2016) 1-6.
- [74] H. Drobná, V. Meinhardová, L. Dubnová, K. Kozumplíková, M. Reli, K. Kočí, L. Čapek, Partially Reduced Ni-NiO-TiO₂ Photocatalysts for Hydrogen Production from Methanol–Water Solution, *Catalysts*, 13 (2023) 293.

- [75] M.A. Munawar, A.H. Khoja, M. Hassan, R. Liaquat, S.R. Naqvi, M.T. Mehran, A. Abdullah, F. Saleem, Biomass ash characterization, fusion analysis and its application in catalytic decomposition of methane, *Fuel*, 285 (2021) 119107.
- [76] M.M. Treacy, J.B. Higgins, *Collection of simulated XRD powder patterns for zeolites fifth (5th) revised edition*, Elsevier 2007.
- [77] M. Tsujiguchi, T. Kobashi, M. Oki, Y. Utsumi, N. Kakimori, A. Nakahira, Synthesis and characterization of zeolite A from crushed particles of aluminoborosilicate glass used in LCD panels, *Journal of Asian Ceramic Societies*, 2 (2014) 27-32.
- [78] M. Tassopoulos, R.J.Z. Thompson, Transformation behaviour of zeolite A to hydroxysodalite in batch and semi-batch crystallizers, 7 (1987) 243-248.
- [79] W. Kim, D. Choi, S. Kim, Sonochemical synthesis of zeolite A from metakaolinite in NaOH solution, *Materials transactions*, 51 (2010) 1694-1698.
- [80] S.M. Pandharkar, S.R. Rondiya, A.V. Rokade, B.B. Gabhale, H.M. Pathan, S.R. Jadhkar, Synthesis and characterization of molybdenum back contact using direct current-magnetron sputtering for thin film solar cells, *Frontiers in Materials*, 5 (2018) 13.
- [81] S. Naghdi, K.Y. Rhee, M.T. Kim, B. Jaleh, S.J. Park, Atmospheric chemical vapor deposition of graphene on molybdenum foil at different growth temperatures, *Carbon letters*, 18 (2016) 37-42.
- [82] S. Kowalak, A. Jankowska, E. Mikołajska, Using of zeolite LOS for preparation of sulfur pigments, *Microporous and mesoporous materials*, 127 (2010) 126-132.
- [83] W. Mozgawa, M. Król, J. Dyczek, J. Deja, Investigation of the coal fly ashes using IR spectroscopy, *Spectrochimica Acta Part A: Molecular and Biomolecular Spectroscopy*, 132 (2014) 889-894.
- [84] J. Kalembkiewicz, D. Galas, E. Sitarz-Palczak, The Physicochemical Properties and Composition of Biomass Ash and Evaluating Directions of its Applications, *Polish Journal of Environmental Studies*, 27 (2018).
- [85] N.M. Musyoka, L.F. Petrik, W.M. Gitari, G. Balfour, E. Hums, Optimization of hydrothermal synthesis of pure phase zeolite Na-P1 from South African coal fly ashes, *Journal of Environmental Science and Health, Part A*, 47 (2012) 337-350.
- [86] N. Omisanya, C. Folayan, S. Aku, S. Adefila, Synthesis and characterisation of zeolite a for adsorption refrigeration application, *Advances in Applied Science Research*, 3 (2012) 3746-3754.
- [87] J. Cao, Q. Sun, P. Wang, J. Shen, X. Dai, Synthesize and characterize of Fe₃O₄/zeolite 4A magnetic nanocomposite, *Journal of Dispersion Science and Technology*, 43 (2022) 517-525.

- [88] A. Fernández-Jiménez, A. Palomo, Mid-infrared spectroscopic studies of alkali-activated fly ash structure, *Microporous and mesoporous materials*, 86 (2005) 207-214.
- [89] D. Chen, M. Liu, L. Yin, T. Li, Z. Yang, X. Li, B. Fan, H. Wang, R. Zhang, Z. Li, Single-crystalline MoO₃ nanoplates: topochemical synthesis and enhanced ethanol-sensing performance, *Journal of Materials Chemistry*, 21 (2011) 9332-9342.
- [90] L. Gomathi Devi, B. Narasimha Murthy, Characterization of Mo doped TiO₂ and its enhanced photo catalytic activity under visible light, *Catalysis letters*, 125 (2008) 320-330.
- [91] A. Naveed, R.A. Khera, U. Azeem, I. Zubair, A. Farhat, A.R. Ayub, J. Iqbal, Tuning the optoelectronic properties of benzodithiophene based donor materials and their photovoltaic applications, *Materials Science in Semiconductor Processing*, 137 (2022) 106150.
- [92] Y. Liu, Y. Lv, Y. Zhu, D. Liu, R. Zong, Y. Zhu, Fluorine mediated photocatalytic activity of BiPO₄, *Applied Catalysis B: Environmental*, 147 (2014) 851-857.
- [93] J. Haddad, B. Krogmeier, B. Klingebiel, L. Krückemeier, S. Melhem, Z. Liu, J. Hüpkens, S. Mathur, T. Kirchartz, Analyzing interface recombination in lead-halide perovskite solar cells with organic and inorganic hole-transport layers, *Advanced materials interfaces*, 7 (2020) 2000366.
- [94] J. Wang, H. Song, P. Dong, Z. Zhao, Y. Zhang, Dual fluorescence properties and enhanced thermal stability of SrSi₂O₂N₂: Eu²⁺ phosphors by coupling with gC₃N₄, *RSC advances*, 13 (2023) 6442-6452.
- [95] V. Stengl, S. Bakardjieva, Molybdenum-doped anatase and its extraordinary photocatalytic activity in the degradation of orange II in the UV and vis regions, *The Journal of Physical Chemistry C*, 114 (2010) 19308-19317.
- [96] Q. Zhang, J. Li, M. Xu, Ag decorated ZnO based nanocomposites for visible light-driven photocatalytic degradation: basic understanding and outlook, *Journal of Physics D: Applied Physics*, (2022).
- [97] Q. Wang, K. Domen, Particulate photocatalysts for light-driven water splitting: mechanisms, challenges, and design strategies, *Chemical Reviews*, 120 (2019) 919-985.
- [98] C. McCullagh, N. Skillen, M. Adams, P.K.J. Robertson, Photocatalytic reactors for environmental remediation: a review, *Journal of Chemical Technology & Biotechnology*, 86 (2011) 1002-1017.
- [99] R. Nagarjuna, S. Challagulla, N. Alla, R. Ganesan, S. Roy, Synthesis and characterization of reduced-graphene oxide/TiO₂/Zeolite-4A: A bifunctional nanocomposite for abatement of methylene blue, *Materials & Design*, 86 (2015) 621-626.

- [100] R. Nagarjuna, S. Roy, R. Ganesan, Polymerizable sol-gel precursor mediated synthesis of TiO₂ supported zeolite-4A and its photodegradation of methylene blue, *Microporous and Mesoporous Materials*, 211 (2015) 1-8.
- [101] S. Girma, A.M. Taddesse, Y. Bogale, Z. Bezu, Zeolite-supported g-C₃N₄/ZnO/CeO₂ nanocomposite: Synthesis, characterization and photocatalytic activity study for methylene blue dye degradation, *Journal of Photochemistry and Photobiology A: Chemistry*, 444 (2023) 114963.
- [102] S.A. Mosavi, A. Ghadi, P. Gharbani, A. Mehrizad, Photocatalytic removal of Methylene Blue using Ag@CdSe/Zeolite nanocomposite under visible light irradiation by Response Surface Methodology, *Materials Chemistry and Physics*, 267 (2021) 124696.
- [103] F. Alakhras, E. Alhajri, R. Haounati, H. Ouachtak, A.A. Addi, T.A. Saleh, A comparative study of photocatalytic degradation of Rhodamine B using natural-based zeolite composites, *Surfaces and Interfaces*, 20 (2020) 100611.
- [104] G. Zhang, A. Song, Y. Duan, S. Zheng, Enhanced photocatalytic activity of TiO₂/zeolite composite for abatement of pollutants, *Microporous and Mesoporous Materials*, 255 (2018) 61-68.
- [105] W. Zhang, X. Xiao, L. Zheng, C. Wan, Fabrication of TiO₂/MoS₂@zeolite photocatalyst and its photocatalytic activity for degradation of methyl orange under visible light, *Applied Surface Science*, 358 (2015) 468-478.
- [106] S. Oros-Ruiz, R. Zanella, R. López, A. Hernández-Gordillo, R. Gómez, Photocatalytic hydrogen production by water/methanol decomposition using Au/TiO₂ prepared by deposition-precipitation with urea, *Journal of Hazardous Materials*, 263 (2013) 2-10.
- [107] K. Kočí, M. Reli, M. Edelmannová, I. Troppová, H. Drobná, A. Rokicińska, P. Kuśtrowski, D. Dvoranová, L. Čapek, Photocatalytic hydrogen production from methanol over Nd/TiO₂, *Journal of Photochemistry and Photobiology A: Chemistry*, 366 (2018) 55-64.

LIST OF PUBLICATIONS

Full length article title: Photocatalytic Activity of Molybdenum-Doped-LOS-Zeolite for Efficient Dye Degradation and Hydrogen Production

Journal: Results in Engineering

Impact Factor: 6, Q1 Index

Manuscript number: RINENG_103122

Date of Publication: 15th October 2024







Results in Engineering

Available online 12 October 2024, 103122




In Press, Journal Pre-proof [?](#) [What's this?](#)



Photocatalytic Activity of Molybdenum-Doped LOS- Zeolite for Efficient Dye Degradation and Hydrogen Production


[Hamza Khawaja](#)¹, [Nida Naeem](#)¹, [Asif Hussain Khoja](#)¹  , [Hajirah Kanwal](#)¹, [Ali Raza](#)¹, [Mustafa Anwar](#)², [Rabia Liaquat](#)², [Israf Ud Din](#)³, [Salman Raza Naqvi](#)⁴  , [Abdulaziz Al-Anazi](#)⁵


Show more 

 Add to Mendeley  Share  Cite

<https://doi.org/10.1016/j.rineng.2024.103122> 

[Get rights and content](#) 

[Under a Creative Commons license](#) 

 [open access](#)